THE HYBRID WIND FARM PARAMETERIZATION

by

Yang Pan

A dissertation submitted to the Faculty of the University of Delaware in partial fulfillment of the requirements for the degree of Doctor of Philosophy in Ocean Engineering

Summer 2018

THE HYBRID WIND FARM PARAMETERIZATION

by

Yang Pan

Approved: ____
Mark A. Moline, Ph.D.
Director of the School of Marine Science and Policy

Approved: ____
Estella Atekwana, Ph.D.
Dean of the College of Earth, Ocean, and Environment

Approved: ____
Douglas J. Doren, Ph.D.
Interim Vice Provost for Graduate and Professional Education

I certify that I have read this dissertation and that in my opinion it meets the academic and professional standard required by the University as a dissertation for the degree of Doctor of Philosophy.

Signed: ______________________________

Cristina L. Archer, Ph.D.
Professor in charge of dissertation

I certify that I have read this dissertation and that in my opinion it meets the academic and professional standard required by the University as a dissertation for the degree of Doctor of Philosophy.

Signed: ______________________________

I. Pablo Huq, Ph.D.
Member of dissertation committee

I certify that I have read this dissertation and that in my opinion it meets the academic and professional standard required by the University as a dissertation for the degree of Doctor of Philosophy.

Signed: ______________________________

Brian Hanson, Ph.D.
Member of dissertation committee

I certify that I have read this dissertation and that in my opinion it meets the academic and professional standard required by the University as a dissertation for the degree of Doctor of Philosophy.

Signed: ______________________________

Ruben Delgado, Ph.D.
Member of dissertation committee

ACKNOWLEDGEMENTS

Thank you to the School of Marine Science and Policy for offering me the chance to study and work as a Ph.D. student in such a nice place. Thank you to my advisor Dr. Cristina Archer, who trusted me to work independently on the amazing projects. Dr. Archer is a knowledgeable expert and a trustable friend, who provided valuable guidance. Thank you for your time in the past four years for siting down with me to discuss my research whenever I need. I would like to thank my committee members Dr. I. Pablo Huq, Dr. Brian Hanson and Dr. Ruben Delgado for their insights and assistance to my research and dissertation. Thank you to Delaware Municipal Electric Corporation and Magers Family for the fellowship. It's your generous financial assistance that help me to continue my research and finish my dissertation. I also appreciate the support of my colleagues Dr. Chi Yan, Dr. Shengbai Xie and Dr. Niranjan Ghaisas, who have provided valuable experiences in computational fluid dynamics. Most importantly, it is by the love and support of my family, especially my wife, that I was able to complete my papers and dissertation. I would like to tribute this work to my wife, and our new born daughter.

TABLE OF CONTENTS

LIST OF TABLES

LIST OF FIGURES

ABSTRACT

The goals of this research are to improve the current treatment of wind farms in large-scale models via a new hybrid wind farm parameterization to better understand the potential impacts of offshore wind farms on the environment.

Wind turbines extract energy from the atmosphere and the resulting wakes affect the boundary layer and the environment. The approach chosen in this dissertation to study these impacts of wind turbines is numerical simulations utilizing the weather prediction model called Weather Research and Forecast (WRF), in which wind farms are currently parameterized as simple elevated sinks of kinetic energy and sources of turbulent kinetic energy (TKE). A well-developed wind farm parameterization is essential to better understand the potential impacts of wind farms on weather and climate at the regional to global scales.

The first part of this dissertation is therefore a case study to understand the impacts of hypothetical, large, offshore wind farms on local meteorology, especially the precipitation, employing the current two most widely used wind farm parameterizations. This study quantitatively tests whether the offshore turbines may affect precipitation patterns during Hurricane Harvey, since Hurricane Harvey brought to the Texas coast possibly the heaviest rain ever recorded in U.S. history, which then caused flooding at unprecedented levels. Model results indicate that the offshore wind farms have a strong impact on the distribution of accumulated precipitation, with an obvious decrease onshore, downstream of the wind farms, and an increase in the offshore areas, upstream of or within the wind farms. The accumulated precipitation during Harvey was reduced by up to 21% in the presence of offshore wind farms consisting of hundreds of thousands of turbines. Compared with the control case with no wind turbines, increased horizontal wind divergence and lower vertical velocity are found where

the precipitation is reduced onshore, whereas increased horizontal wind convergence and higher vertical velocity occur upstream or within the offshore wind farms. The sensitivity to the size of the offshore array, the inter-turbine spacing, and the details of the wind-farm parameterization is assessed.

In the second part of this dissertation, a new hybrid wind farm parameterization (a.k.a. hybrid model) is developed, which is not based on physical processes or conservation laws, but on a multiple linear regression of the results of sophisticated, high-resolution large-eddy simulations (LES) with simple geometric properties of the wind farm layout. The need for the new hybrid model arises from three previously-unknown weaknesses in the current wind farm parameterization in WRF, i.e., it neglects the effects of wind direction, it is insensitive to the relative position of the wind turbines within the farm, and it injects excessive TKE in the atmosphere. The new hybrid parameterization, however, successfully remedies these weaknesses. After validations against observations collected at an existing offshore wind farm (Lillgrund in Sweden) and against LES results at three hypothetical wind farms, the wind speed deficit and TKE predicted with the hybrid model are found to be in excellent agreement with the LES results and the wind power production estimated with the hybrid model also performs well compared with the observation data. In conclusion, wind turbine position, wind direction, and added TKE are essential to properly model wind farm effects on the surroundings and the hybrid wind farm parameterization is a promising tool to incorporate them in meso- and large-scale simulations.

Chapter 1

INTRODUCTION

The energy demand is growing rapidly and the world energy consumption is projected to increase 48% between 2012 and 2040 (U.S. Energy Information Administration, 2016). The supply of the traditional fossil fuels, such as the coal, oil and gas, is limited and the use of these fuels, may be damaging to the environment.Unlike fossil fuel, wind energy will not run out and is a low or carbon-free emission energy source. As a source of clean, cheap and efficient energy, wind energy has been expanding globally and has become the fastest renewable energy technology. With 8.7 gigawatts (GW, 10^9 Watts) of new installed capacity in 2016, the increase of new onshore wind installations exceeded the construction of all other forms of electricity in 2016 (U.S. Energy Information Administration, 2017).

Wind farms often consist of wind turbines positioned in several rows and columns. Wind turbines in the wind farm extract the kinetic energy from the atmosphere and convert it to electric power. A wake is generated by each wind turbine, which is a plume-like volume downwind of wind turbines characterized by a lower wind speed and increased turbulence intensity. Wake propagates downward along the rows and can cause a severe power reduction (wake losses) at downstream turbines. The wake losses or wake effects has been the topic of many studies (Sorensen and Nielsen, 2006; Archer et al., 2013; Wu and Porté-Agel, 2013; Stevens et al., 2014; Ghaisas and Archer, 2016; Pan and Archer, 2018). In additon to the wake effects, as the wind turbines extract energy from the atmosphere, the wind farm may also affect the atmospheric boundary layer. The influence of the wind farms on the atmospheric boundary layer includes changes in the near-surface properties, such as near-surface temperature, humidity and surface fluxes.

In a high resolution numerical study based on the large eddy simulation (LES), a computational technique for simulating turbulent flows, warming was found below the rotor area in stable conditions (Lu and Porté-Agel, 2011); however, warming was also found in a convective boundary layer (Lu and Porté-Agel, 2015). Another LES study (Calaf et al., 2010) found an overall increase in the scalar surface fluxes of about 10-15% in the presence of an infinite wind turbine array. Apart from the numerical simulations described above, field data and observations are also used to evaluate the impacts of wind farms on the surface properties. Baidya Roy and Traiteur (2010) found warming during the night and cooling during the day, and was the first to provide observational evidence of meteorological impacts of wind farms. Zhou et al. (2012) examined the satellite data and found warming both during the night and day over wind farms in contrast with the nearby non-wind-farm regions. Observations of a large wind farm showed a near-surface warming around 1.5K in the direct wake during the night (Smith et al., 2013). Two recent field campaigns the Crop Wind Energy Experiment (CWEX 2010 and 2011) were done in Iowa, and weak warming was found near the surface in the far wake (at 35 rotor diameters) for all atmospheric stabilities (Rajewski et al., 2013). The impact on the sensible heat fluxes is found to be small and the flux of water can be enhanced in the wake of the turbines. An unprecedented drought in Mongolia was also reported within the turbine areas.(Abbasi et al., 2016). Wind tunnel experiments implemented by Zhang et al. (2013) showed an overall mean reductions in sensible heat flux less than 4%. In addtion to changes in surface properties, it has been shown that large wind farms can also influence the structure of the boundary layer, such as boundary layer depth and wind direction (Johnstone and Coleman, 2012; Abkar and Porté-Agel, 2013).

These studies above confirmed that the presence of wind farms can alter the lower boundary layer, and affect the meteorology and environment at the local scale. As the scales of wind farms grow, the massive deployment of wind energy in large-scale wind farms could affect the meteorology and climate from the local scale to the regional, and even the global scale. Most of the investigations into the potential impacts of the large-scale wind farms have taken the form of numerical studies since few observations exist. At the regional or global scale, the mesoscale or climate models have been employed, using two types of approaches to parameterize the effects of wind farms: 1) wind farms are implicitly represented as enlarged surface aerodynamic roughness length; 2) wind farms are represented as elevated momentum sinks and sources of turbulent kinetic energy sources. Models using modified surface roughness to represent wind farms found both warming and cooling near the surface (Kirk-Davidoff and Keith, 2008; Wang and Prinn, 2010) or warming (Miller et al., 2011). Other studies based on the method of a momentum sink and a source of turbulence reported warming (Adams and Keith, 2013), cooling (Jacobson and Archer, 2012), warming in stable and cooling in unstable atmospheric conditions (Baidya Roy et al., 2004), or warming in a stable atmosphere and little temperature change in an unstable atmosphere (Fitch et al., 2013a)

Thus it is of great scientific importance to quantify how the large scale extraction of energy from the wind affects local, regional or global meteorology and climate. At coarse regional or global scales, few observations exist and the proposed deployment of wind power is hypothetical. A numerical model with realistic meteorological data input, such as the mesoscale model Weather Research Forecast (WRF) model and climate model the Community Atmosphere Model (CAM), is still an important tool to better capture interactions between the wind turbines and the atmospheric boundary layer. The approaches employed in both models to represent the effects of wind farms, as mentioned above, are essential to simulate the interactions between wind farms and the atmospheric boundary layer. Thus, developing and testing an improved wind farm parameterization to better understand the effects of large wind farms is the primary focus of the research work. The study is organized as two separate chapters:

Chapter 2 evaluated the impacts of large-scale wind farms on local weather conditions through a case study of Hurricane Harvey, employing the current most widely used Fitch wind farm parameterization (Fitch et al., 2012) and the elevated surface roughness method. Many studies have reported surface temperature changes in the presence of wind farms, but very few studies have focused on the impacts of precipitation (Wang and Prinn, 2010; Fiedler and Bukovsky, 2011; Marvel et al., 2013a; Vautard et al., 2014; Fitch, 2015; Possner and Caldeira, 2017), which have shown the changes in mean precipitation of 1% to 10%. The changes were not significant since the focus were on the climate and the results were averaged over many years. Fiedler and Bukovsky (2011) claimed that precipitation may be significantly altered during tropical events in the summer in Gulf of Mexico, but the accuracy of the simulation was not validated. Although hurricane-prone regions, such as the Gulf Mexico or the U.S. east coast, are often not considered for offshore wind development because of the high risk of damage to the wind turbines, in the past few years there has been a growing interest by the wind industry in designing stronger wind turbines that can withstand the high winds during hurricanes. As such, it is important to understand what impacts such offshore wind farms could have on local weather conditions during hurricanes. Moreover, with stronger wind speed during hurricanes, more energy are extracted from the atmosphere and thus the impacts of wind farms on the environment may be stronger in a short term. A recent modeling study (Jacobson et al., 2014) suggests that large arrays of offshore wind farms may mitigate extreme weather conditions, such as the wind speed and storm surge, where the scenario of more than 70,000 wind turbines placed along the coast of the city of New Orleans was investigated. However, the impacts on the precipitation pattern were not reported.

In this chapter Hurricane Harvey was chosen here to study precipitation effects since it has brought heavy rain and severe flooding damage to Texas and thus is an ideal case to evaluate the impacts of large-scale wind farms on precipitation. Weather research forecast (WRF) model was employed to simulate the Hurricane Harvey. A series of simulations with different layout setups were run to to evaluate the potential changes in precipitation. The changes in precipitation are illustrated and the potential mechanism behind these changes were analyzed. Sensitivity tests of different layouts, wind farm locations, and parameterizations are also presented in this chapter, which is adapted from a research paper currently under review in Environmental Research

Letters.

The wind farm simulations of Hurricane Harvey presented in Chapter 2 is modeled using the standard Fitch wind farm parameterization (Fitch et al., 2012) and the elevated surface roughness method. The later method extracted the kinetic energy near the surface and has shown to be insufficient to capture the characteristics of turbine-induced flow (Jacobson and Archer, 2012; Fitch et al., 2013a). The Fitch parameterization are more advanced and widely used. However, this parameterization, as well as other previous wind farm models (Baidya Roy et al., 2004; Blahak et al., 2010; Jacobson and Archer, 2012; Volker et al., 2015; Vollmer et al., 2016), does not consider the effects of wind direction and wind farm layout within a grid cell. All the wind turbines within the same grid cell are considered identical, regardless of their position in the layout. This simplified method treats all the turbines in the single grid cell as the front-row turbine and thus it ignores the actual wind speed and power reductions of turbines in the following rows. Furthermore, the amount of added turbulent kinetic energy (TKE) induced by the wind turbines is not calculated correctly.

In all the models above, due to the coarse resolution, it is typical that several wind turbines may fall into one grid cell. Every turbine may encounter different local upstream inflow depending on its position in the layout and the upstream wind direction. However, in the models above, all the turbines in a grid cell are considered exactly the same (same location and same upstream wind speed) and the grid average value is only the superposition of a series of identical values. In other word, all the models failed to consider the effects of the wind farm layout and wind direction in a grid cell. So the grid velocity used to estimate the drag forces induced by the turbines, is not accurate since the effects of layout within one grid are not included. However, the wind direction and wind farm layout is both critical, because wakes of the upstream turbines can lead to significant power reductions (Archer et al., 2013; Ghaisas and Archer, 2016). The Fitch model, mentioned above, have over-predicted the power output compared with both the LES and the experimental wind farm data (Eriksson et al., 2015). In an attempt to improve the parameterization (Abkar and Porté-Agel, 2015), the results of LES were used to calibrate the model and good agreement were achieved between the model and LES. However, the LES runs have to be carried out prior to every wind farm simulation and the high computational cost made it impossible to simulate a large-scale wind farm or consider potentially different wind farm layouts and wind directions. The results of LES , though, can be used to develop the new wind farm parameterization. It is also interesting to see if the results employing the current wind farm parameterization in mesoscale model or large-scale model, can match the results of LES, when averaged over appropriate length scales.

Chapter 3 proposes a hybrid wind farm parameterization to address these weaknesses described above. The hybrid wind farm parameterization – or hybrid model – utilizes knowledge gained via LES, previously proven to be able to successfully describe local interactions between a wind farm and the atmosphere in a series of studies (Calaf et al., 2010; Churchfield et al., 2012b; Wu and Porté-Agel, 2013; Lu and Porté-Agel, 2015). The few, detailed and fine-scale results like LES, can be used to help us developing the parameterization. In the process incorporating this knowledge, some geometric properties are defined to include the variations in the wind farm layouts and wind directions. Once the model is successfully calibrated with LES results, it is implemented and run in the WRF model. The simulation results were then validated against both the LES results and wind-farm, power-production data. The sensitivity tests are also implemented to ensure the parameterization also works on other wind farms and for different grid sizes. The presentation of this work has been adapted from a research paper published in Boundary-Layer Meteorology.

Chapter 2

PRECIPITATION REDUCTION DURING HURRICANE HARVEY WITH OFFSHORE WIND FARMS

2.1 Introduction

Wind farms provide clean electricity by extracting energy from the wind flow. Since the wind flow is affected during the energy conversion, it is expected that the disturbed wind flow can affect the environment and the local weather, e.g., temperature and precipitation. Both numerical studies (Baidya Roy et al., 2004; Adams and Keith, 2007; Baidya Roy and Traiteur, 2010; Wang and Prinn, 2010; Somnath Baidya, 2011; Fitch et al., 2013a; Lu and Porté-Agel, 2015) and observations (Zhou et al., 2012; Rajewski et al., 2013; Smith et al., 2013; Rajewski et al., 2014) have found surface temperature changes in the presence of wind farms. However, very few studies have focused on the impact of wind farms on precipitation. A numerical study by Wang and Prinn (2010) has found large-scale installation of wind power may lead to alterations of global distributions of rainfall (10% in some areas). Another study Fiedler and Bukovsky (2011) found that, although an onshore wind farm may have a strong impact on precipitation during one season, only a slight impact, not statistically significant, was detected over a 62-seasons average. At the scale of global energy demand(Marvel et al., 2013a), decreases in zonal mean precipitation of 1% were reported. A regional modeling study (Vautard et al., 2014), found a statistically significant signal only in winter, with changes with in 0-5% for precipitation. Fitch (2015) found the impacts resulting from a global deployment of large-scale wind farms are negligible, with a slight increase in precipitation over the wind farm areas. A recent study (Possner and Caldeira, 2017) modeled large-scale wind farms both in the open ocean and on the land, and found no statistically significant changes in surface precipitation.

In this study, we assess whether a large array of offshore wind farms can inadvertently impact precipitation during severe weather conditions like hurricanes. In the literature, Jacobson et al. (2014) have shown offshore wind farms can reduce wind speed and storm surge during hurricanes, but did not assess the impact on precipitation. Fiedler and Bukovsky (2011) claimed that precipitation during a few tropical cyclones in the Gulf of Mexico were significantly altered by the presence of inland wind farms; however, the wind farms were far from the evaluated areas and the forecast accuracy of the simulations was not validated. Moreover, the simulation results were for a whole summer season, which is inadequate to prove the impacts are mostly within the tropical events, which usually last a few days. In this study, the case study of Hurricane Harvey is chosen since it brought to the Texas coast possibly the heaviest rainfall on record and caused severe flood damage to the metro-Houston areas. The effects on precipitation may be easier to be detected with large amount of rainfall, and thus it is an ideal case to study precipitation. The Weather Research Forecast model version 3.6 is employed to simulate Hurricane Harvey. The Advanced Reseach WRF version is used instead of the hurricane version HWRF with data assimilation. Although the latter has shown superior performance in previous studies of hurricanes (Dodla et al., 2011), the goal of this study is not to simulate Hurricane Harvey perfectly, but rather to simulate the impacts of future offshore wind farms as realistically as possible. Assimilating observations that were collected in the absence of such wind farms would not be realistic in simulations that include the wind farms, therefore ARW was run without data assimilation and without the complex data-driven vorticity enhancements used in HWRF. The simulation results without wind farms are validated with observations, including hurricane track, minimum sea-level pressure, wind field and precipitation in Houston, in order to ensure a reasonably accurate forecast. The wind farms are modeled using the Fitch parameterization (Fitch et al., 2012), which is the most widely used wind-farm parameterization in mesoscale models. An additional case, which used the enhanced surface roughness method to represent the effects of the wind farms, was also simulated, to verify the sensitivity to wind-farm parameterization.

2.2 Simulations

In this section, the details of the simulations and the validation against observations are presented.

2.2.1 Setup

The model domain is set up to cover the coast of Texas and Louisiana, as shown in figure 2.1. The horizontal resolution is $\Delta x = \Delta y = 10.667$ km. The initial and boundary condition data are taken from the North American Mesoscale Forecast System (NAM) with a resolution of 12 km. The model is integrated for four days from 0000 UTC August 25, 2017 to 0000 UTC August 29, 2017 with a 6 hour spin-up. The 1.5-order, 2.5-level MYNN PBL scheme (Nakanishi and Niino, 2009) is selected since the wind-farm parameterization is dependent on this scheme and it is widely used in the literature (Fitch et al., 2013b; Volker et al., 2015; Eriksson et al., 2015). The Kain–Fritsch convective parameterization scheme (Kain and Fritsch, 1992; Kain, 2004) is used to predict the convective component of precipitation and the land-surface model is Noah (Ek et al., 2003). The details of the simulation setup are presented in Table 2.1.

Number of grid points	NX=155, NY=122, NZ=41
Horizontal grid spacing	10.667 km
PBL scheme	MYNN
Surface Layer scheme	MYNN
Land surface model	Noah
Cumulus scheme	Kain-Fritsch
wind-farm parameterization	Fitch

Table 2.1: Summary of the WRF model settings used in the simulations.

The wind farms are modeled using the Fitch wind-farm parameterization (Fitch et al., 2012), which models the wind farms as a momentum sink and an added turbulence kinetic energy (TKE) source. The magnitude of the drag force on the atmosphere

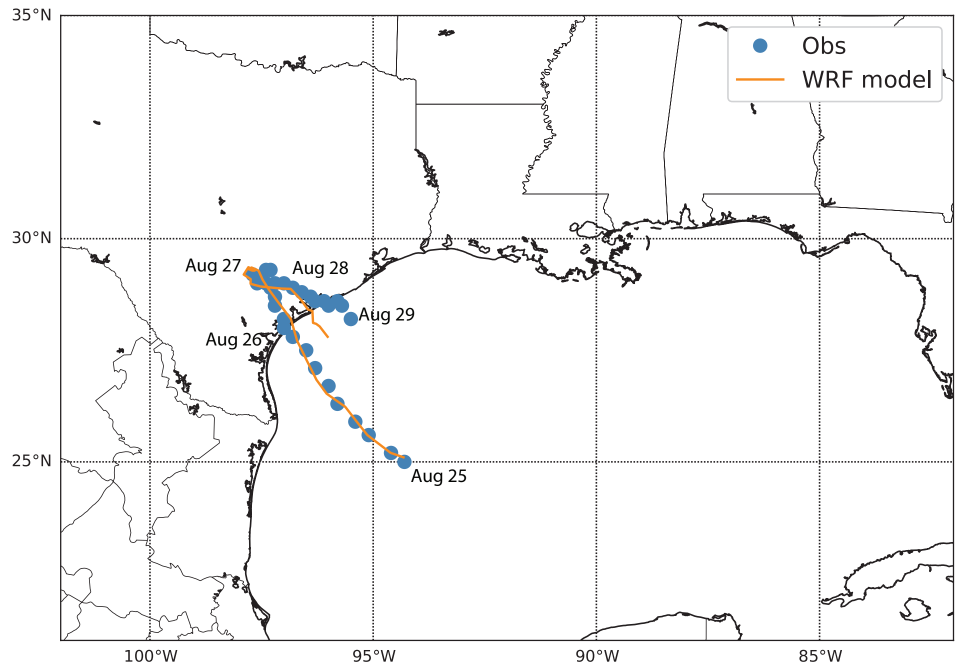

Figure 2.1: The model domain used in this study, with Hurricane Harvey's track from observations and from the CTRL simulation.

induced by one wind turbine can be expressed as:

$$F = \frac{1}{2} C_T(V) \rho V^2 A, \tag{2.1}$$

where V is the horizontal wind speed over the disk, C_T is the thrust coefficient, ρ is the air density, and A is the disk area swept by the turbine rotor. The the rate of loss of kinetic energy in the wind $\frac{\partial KE}{\partial t}$ is therefore:

$$\frac{\partial KE}{\partial t} = \frac{1}{2} C_T(V) \rho V^3 A. \tag{2.2}$$

The extracted kinetic energy in the wind goes into the electric power (via a power coefficient) and additional turbulent kinetic energy (via a TKE coefficient). The energy loss induced by heat via friction and mechanical losses are ignored.

The other approach employed to parameterize the wind farms is to increase surface roughness, which was first introduced by Keith et al. (2004). Although the surface roughness parameterization is overly-simplified, as wind turbines extract energy not near the surface, but rather around the rotor disk, it is computationally efficient and therefore it has been used extensively in large-scale simulations of wind farms (Kirk-Davidoff and Keith, 2008; Barrie and Kirk-Davidoff, 2010; Wang and Prinn, 2010; Miller et al., 2011). In this study, the surface roughness parameterization is used to model a supplemental case for sensitivity purposes, aimed at demonstrating that the conclusions derived from our study are robust and do not depend on the exact implementation of the wind-farm parameterization.

A control case with no wind farms, denoted as CTRL, is setup to ensure the accuracy of the simulations and highlight the precipitation differences induced by the turbines under the same model configurations. Five additional cases with different layouts are run next (details in Table 2.2). For all cases, the turbines are installed in waters up to 200 m in depth, due to the technical difficulty and high construction costs in deeper water areas. The wind turbine model is the 7.5-MW Enercon 126 with a diameter D =126 m. To study the best wind farm location, three basic cases (LWF, MWF, SWF for large, medium, and small wind farm), shown in figure 2.2, are modeled that cover differently sized offshore areas, but with the same inter-turbine spacing. Two additional cases cover the same areas as MWF, but with tight (MWF-TS) and wide (MWF-WS) inter-turbine spacings. For all the wind farm cases except SWF, all the turbines were placed along the coast, ranging from the coastline to 100 km offshore (including the bay areas). The SWF case is similar to the MWF case, but only the turbines within the commercial lease zone from the Bureau of Ocean Environment and Management (BOEM) are modeled, in order to avoid the non-construction areas and achieve a more realistic configuration. In this case, there are no turbines modeled close to the coast and in the Galveston Bay (figure. 2.2 c). A supplemental case (MWF-Z0) is modeled with the same setup as MWF but with an increased surface roughness $z0 = 0.5$ m over the turbine areas. The surface roughness value was determined via a series of tests, as described later in Section 2.3.2.

Cases	N.of turbines	Location	Spacing
Control	0	N/A	N/A
LWF	$74,619$	Coast to 100 km	$9D \times 9D$
MWF	$33,363$	Coast to 100 km	$9D \times 9D$
SWF	$28,197$	Within BOEM lease zone	$9D \times 9D$
MWF-WS	$22,242$	Coast to 100 km	$11D \times 11D$
MWF-TS	$59,312$	Coast to 100 km	$7D \times 7D$
MWF-Z0	N/A	Coast to 100 km	N/A

Table 2.2: Summary of the simulation cases. D is the diameter of the wind turbine

2.2.2 Validation

To ensure the accuracy of the simulations, with and without wind farms, the results of the CTRL case (without wind farms) are compared with the observations, including hurricane track, minimum sea-level pressure, maximum wind speed, and precipitation.

The simulated track of Hurricane Harvey agrees well with the observations (The Weather Company (TWC), 2017) prior to August 29, 2017 and is slightly off afterwards

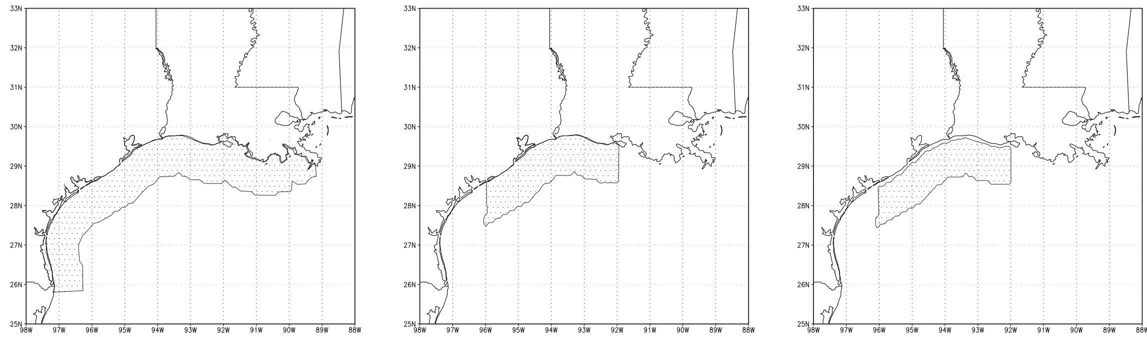

(a) LWF (b) MWF (C) SWF

Figure 2.2: Location of the wind farms in the three layout configurations: a) LWF, b) MWF, and c) SWF

(figure 2.1). Considering that the rainiest days for the metro-Houston area were before August 29, only the results of the first four days will be analyzed in this study. The time series of maximum wind speed, minimum sea-level pressure, and total precipitation during the four days prior to August 29 show a good level of accuracy considering that no observations were assimilated into the simulation (figure 2.3). The modeled minimum sea-level pressure (figure 2.3b) generally follows the trend of the observations, except for an underestimate at the time when the hurricane was strongest. However, the timing of the lowest minimum coincides almost perfectly with the observations.

In order to validate the precipitation predictions, simulated values were extracted at a grid point located downtown Houston from the model domain. Data from 15 gauges from Harris County Flood Control System (Flood Warning System (FWS), 2017) located within the downtown grid point were averaged to make the simulation results and observation data comparable. The simulation results generally underestimated precipitation (figure 2.3c), but most of the times the results are within the error bars. The timings of the two peaks between August 27 and 29 are both close to the observed. The discrepancy between the model results and the observations is possibly due to the lack of vortex initialization and data assimilation, which have been proven to improve the accuracy of the cyclone track and intensity (Kurihara et al., 1995; Wang, 1998; Cavallo et al., 2013; Zhang et al., 2009, 2011; Hamill et al., 2011) but cannot be used for sensitivity runs as those conducted in this study. Although the magnitude of the prediction is slightly off from the observations, the general trend of the results matches. Thus, the CTRL results can be used as a reference state to further evaluate the impacts of the wind farms.

2.3 Results

2.3.1 Precipitation reduction due to horizontal divergence

The wind-farm parameterization correctly extracts kinetic energy at the wind farm locations, as shown by the horizontal distribution of wind speed at hub height at 0900 UTC on August 25, 2017 (figure 2.4). For the same farm, the wind speed reductions depend on the density of turbines. For example, higher wind speed reductions (and therefore higher energy generation) are achieved in the MWF-TS than in the MWF or MWF-WS cases, due to the the higher number of turbines (59,312 vs. 33,363 and 22,242, respectively).

There has been growing interest in the potential of impacts of large-scale wind farms on temperature and moisture. During the daytime, little changes in temperature and moisture are found (not shown), due to the well-mixed layer, which dominates the impacts of the wind farms. During the night, the condition is still unstable, but the turbulent mixing is much weaker than the daytime. Figure 2.5 shows the difference of the near surface properties between LWF and CTRL, during the night time before the landfall. The evaporation rate over the ocean is proportional to the surface wind speed, so the reduced wind speed within the wake of the wind farm may reduce the evaporation rate and water vapor mixing ratio (Jacobson and Archer, 2012). A decrease of near-surface humidity (figure 2.5a), was found within the wind farm and along the coast areas. The maximum humidity reduction is approximately -0.0015 kg/kg, which is around 6.5% change compared with the case without turbines. As the evaporation rate is reduced, the latent heat flux is weakened for most of the areas with turbines installed (figure 2.5b). The percent change due to the wind turbines can reach up to 20% (≈90 W m^{-2}). During the night, the magnitude of the sensible heat flux is

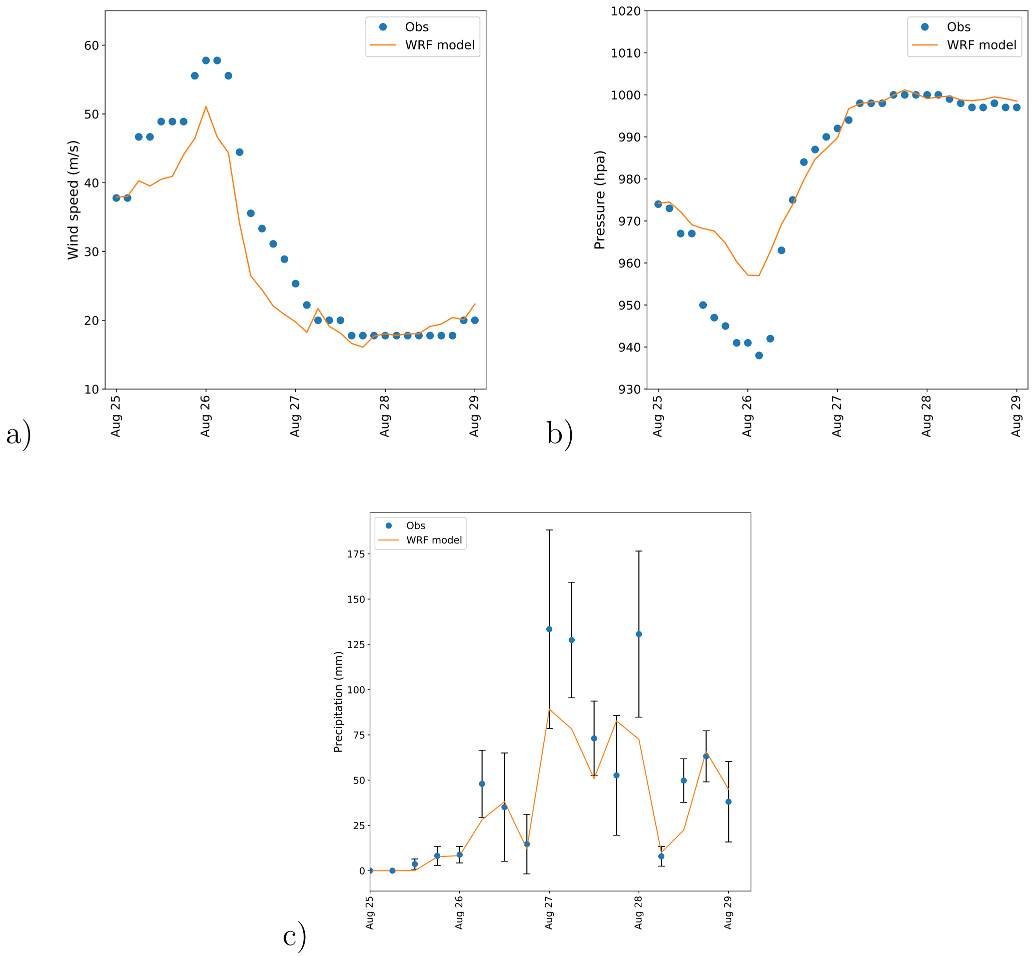

Figure 2.3: Comparison of the CTRL simulation results with observations during Hurricane Harvey: a) hurricane track, b) minimum sea -level pressure, and c) precipitation near downtown Houston.

much smaller compared with the latent heat flux during hurricane, and the changes in sensible heat flux is less than 25 W m^{-2} (figure 2.5c). In the deep wake of the wind farm or near the coastal areas, the sensible heat is weakened, whereas, upstream of the wind farm, the sensible heat flux is strengthened. The weakened upward latent heat flux and sensible heat flux lead to a slight warming up to 1.5 K near the surface (figure 2.5d)

From figure 2.3c, the largest precipitation amounts occurred during the last three days (August 26 to 29) and therefore this time period is selected for further analysis. Looking at 72-hour accumulated precipitation patterns (figure 2.6), both areas with increased precipitation and areas with reduced precipitation are found due to the presence of the wind farms, but not in a random manner. Rather, increased precipitation is found mostly offshore, upstream of or within the wind farms, while reduced precipitation is found onshore or close to the coastline, downstream of the wind farms. Considering the damage caused by precipitation and flooding in the metro-Houston area, this coherent pattern of reduced precipitation onshore suggests that huge potential benefits, in terms of avoided damage and lives saved, could be harnessed by installing large offshore wind farms in the Gulf.

Compared with the MWF case (figure 2.6c), the LWF case (figure 2.6b) produces very similar changes in precipitation patterns, especially along the coast near Houston, even though the latter covers a much larger area and has more than twice the number of wind turbines. The physical mechanisms behind this finding will be explained in the next paragraph, but at the moment it can be concluded that an array of wind farms as large as that in the LWF case is not necessary since it produces little improvement in the benefits with much higher costs than the MWF case. This is the reason that the sensitivity tests to inter-turbine spacings in section 2.3.2 will be based on the MWF case.

To better quantify the changes in precipitation, a sector covering south Houston ($-95.7°$ W to $-95.2°$ W and $29.5°$ N to $29.8°$ N) is selected for further analysis. The

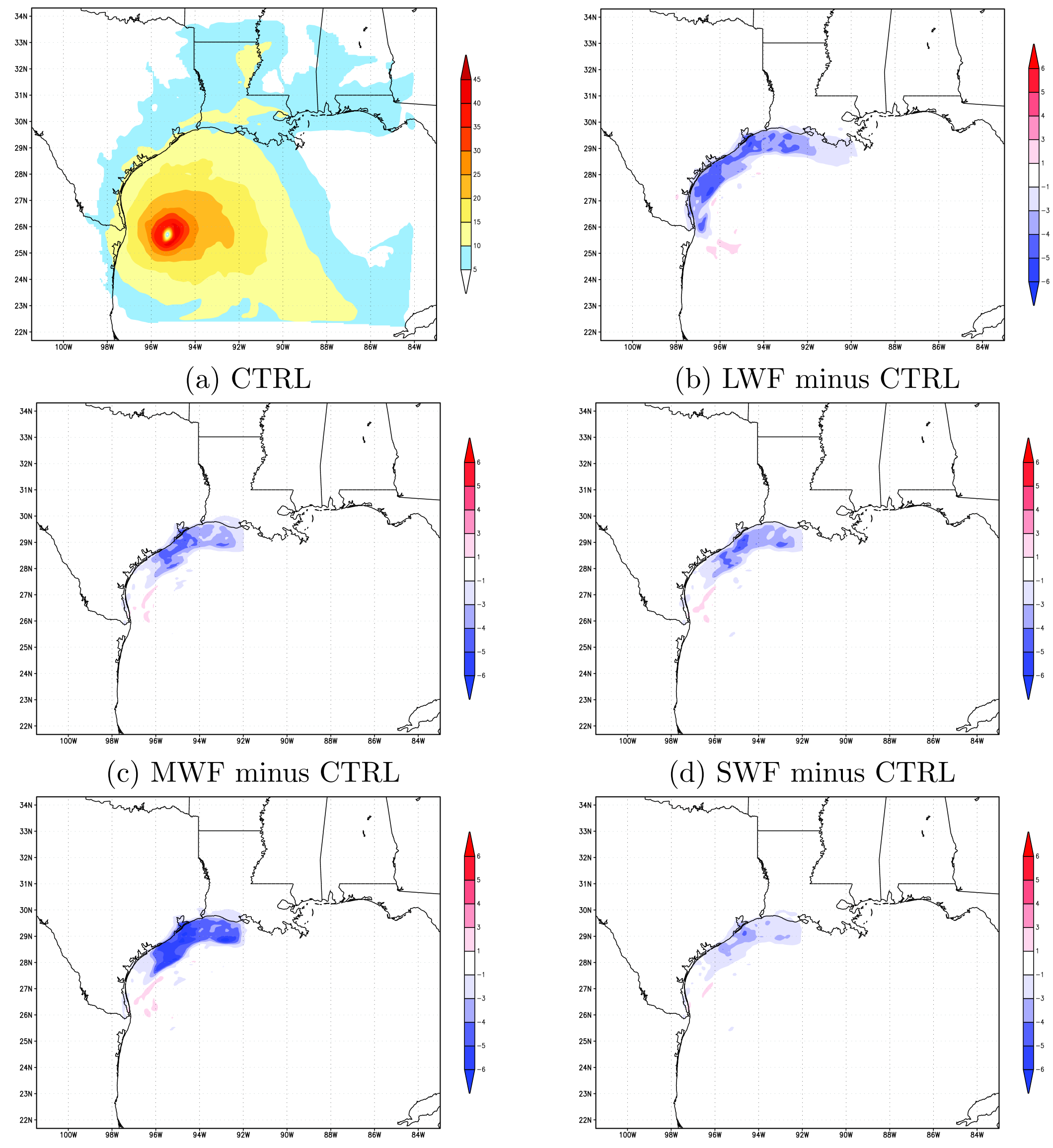

(a) CTRL

(b) LWF minus CTRL

(c) MWF minus CTRL

(d) SWF minus CTRL

(e) MWF-TS minus CTRL

(f) MWF-WS minus CTRL

Figure 2.4: Hub-height winds speed results at 0900 UTC August 25, 2017: a) wind speed (m/s) in CTRL case; and b-f) wind speed difference (m/s) between the cases indicated in the figure labels and CTRL.

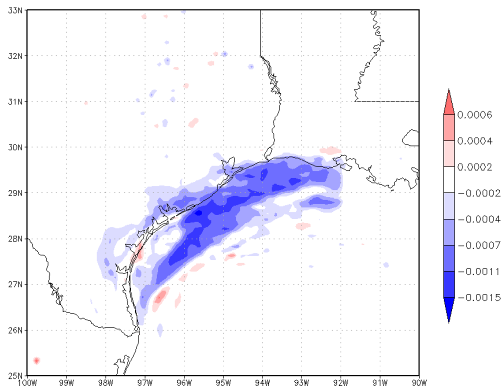

(a) Near-surface Humidity (kg kg^{-1})

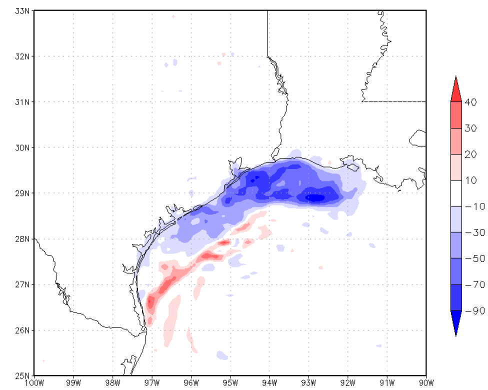

(b) Latent heat flux (W m^{-2})

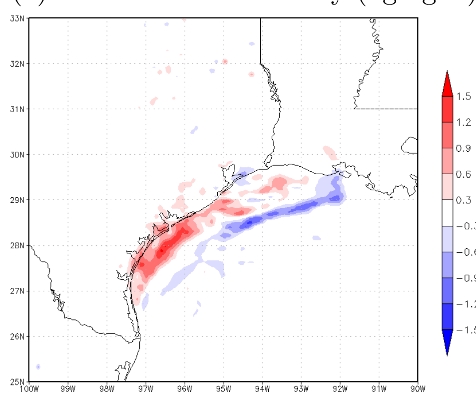

(c) Near-surface temperature (K)

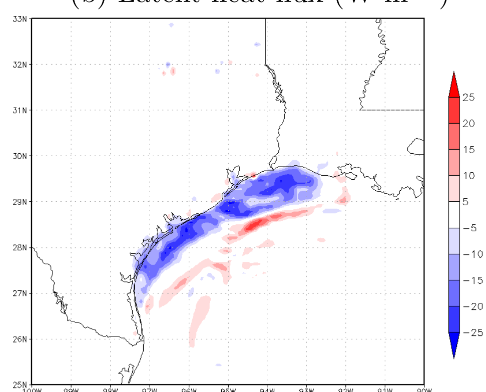

(d) Sensible heat flux (W m^{-2})

Figure 2.5: Results of surface properties at 0800 UTC August 25, 2017; all the panels show the difference between LWF and CTRL

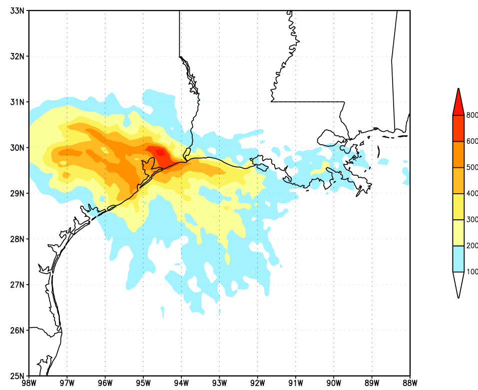

(a) CTRL

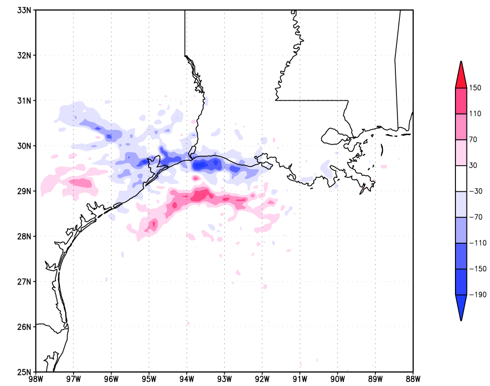

(b) LWF minus CTRL

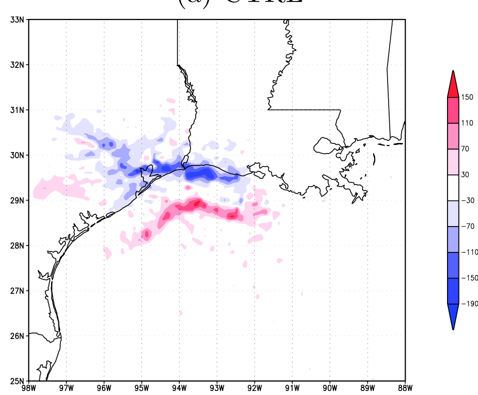

(c) MWF minus CTRL

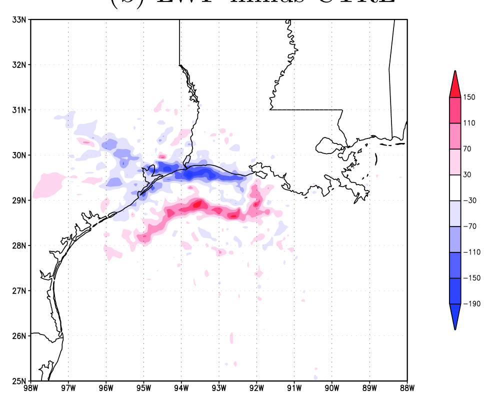

(d) SWF minus CTRL

Figure 2.6: Accumulated precipitation (mm) or precipitation difference (mm) during 26-29 August 2017: a) CTRL, b) MWF minus CTRL, c) LWF minus CTRL, and d) SWF minus CTRL.

simulated precipitation amount is averaged over this sector. The reduction in the 72-hour accumulated precipitation (see Table 2.3) is approximately 15% for both the MWF and LWF case. For the SWF case, the reduction is only about 10%, which suggests that the wind farms placed in the Galveston Bay areas, missing in SWF, could be of great importance for the city of Houston.

The hypothesis put forward here is that changes in precipitation – increases offshore and decreases onshore – are associated to changes in horizontal wind divergence and in vertical wind speed caused by the wind farms. To verify this hypothesis, the difference between these two terms in the LWF case minus the CTRL case at landfall are shown in figure 2.7. To the northeast of the hurricane center, the wind is blowing from the sea towards the land. In these areas, the horizontal wind divergence difference (LWF minus CTRL in figure 2.7a) is negative upstream of the wind farms, as the wind slows down because of the presence of the wind farms, and is positive downstream of the wind farms, as the wind speed recovers past the wind farms. Correspondingly, the vertical wind speed difference (figure 2.7b) is positive upstream of the wind farms, meaning that upward motion is enhanced and therefore precipitation is increased, and negative downstream of the wind farms, meaning that upward motion is suppressed and therefore precipitation is reduced. To the south of the hurricane center, the wind is coming from the shore, so changes in the horizontal wind divergence and vertical wind speed are opposite to those to the northeast of the hurricane center. However, over the entire 3-day period, no substantial changes in precipitation were found in these areas.

2.3.2 Sensitivity analysis

To assess the sensitivity to inter-turbine spacing and parameterization formulation, the focus of this section will be on the 24-hour accumulated precipitation from 26 to 27 August 2017, during which the winds were strongest and the effects of the wind farms on precipitation were more pronounced (figure 2.6c vs. figure 2.8a). From the 24-hour accumulated precipitation difference between the wind farm cases with various inter-turbine spacings and the MWF case with no wind turbines (figure 2.8), obvious

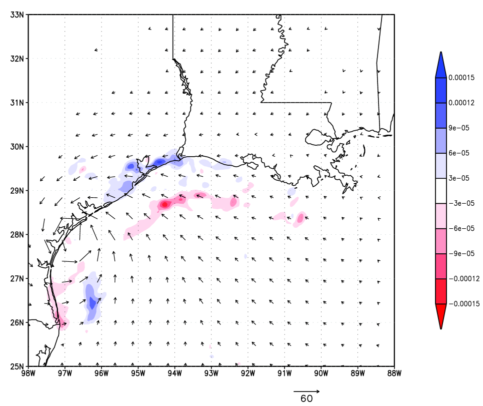

(a) DIVG

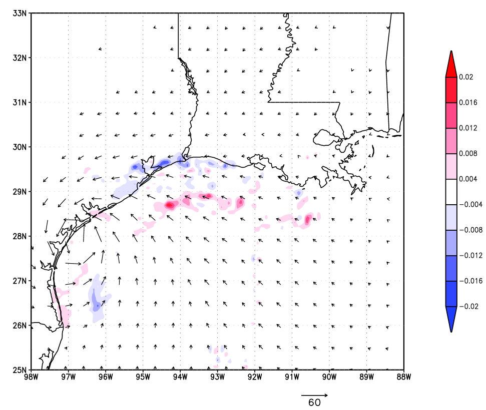

(b) Vertical wind speed

Figure 2.7: Results at the hub height at landfall a) Horizontal divergence difference (1/s) LWF minus CTRL, b) vertical wind speed difference (m/s) LWF minus CTRL

precipitation reductions onshore can be noticed. The compact case (figure 2.8b), with more turbines than the MWF case (figure 2.8a), exhibits a stronger reduction in precipitation inland and a stronger increase in precipitation offshore and over larger areas. Vice versa, in the wide-spacing case MWF-WS (figure 2.8c), the precipitation changes are qualitatively the same, but smaller in magnitude and aerial extent.

In addition to the wind farm cases modeled with the Fitch wind-farm parameterization, case MWF-Z0 was run with a different treatment of the effect of the wind farms, namely, an increase in the value of surface roughness z_0 only over the wind farm area. Although overly simplified, as wind farms are elevated, not surface-based, drag elements (Fitch et al., 2013b; Jacobson and Archer, 2012), increasing surface roughness is a treatment of wind farms used in many studies in the past Keith et al. (2004); Kirk-Davidoff and Keith (2008); Barrie and Kirk-Davidoff (2010); Wang and Prinn (2010); Miller et al. (2011). There is not a well-established method to determine by how much surface roughness should be increased to better represent the effect of the wind farms. In the literature, a series of values ranging from 0.12 m to 3.4 m values have been proposed (Calaf et al., 2010; Wang and Prinn, 2010; Jacobson and Archer, 2012; Fitch et al., 2013b). Here we tested several values between 0.2 m and 0.8 m and compared the resulting wind speed profiles averaged over the wind farm area to identify which gave a distribution of wind speed around hub height that was closest to that of the MWF case. The selected value of surface roughness is 0.5 m and the case is named MWF-Z0.

Results from MWF-Z0 confirm that precipitation is reduced inland and increased offshore, with a spatial pattern overall similar to that of the previous cases (figure 2.8d), although closest to the results from the case with tight inter-turbine spacing (MWF-TS in figure 2.8b) in terms of magnitude. This suggests that using an increased value of surface roughness may exaggerate the effects on precipitation overall, although the spatial distribution of the precipitation change was such that the Houston area was less affected with MWF-Z0 and SWF than with the other cases. At the same time, the comparison against the MWF-Z0 results was useful because it confirmed that offshore wind farms can impact the precipitation distribution during a hurricane like Harvey regardless of the details of the wind-farm parameterization used.

To highlight the sensitivity of the precipitation to different layouts and parameterizations, Table 2.3 shows a summary of the precipitation reduction of all the cases in the sector covering south Houston, described previously in section 2.3.1. The LWF and MWF simulations achieve almost the same benefit ($\sim 15\%$), despite the fact that the LWF simulation includes more than twice the number of turbine of MWF. Increasing the number of turbines in the same area as MWF causes a larger reduction in precipitation (MWF-TS: 21.17%) and, vice versa, decreasing the number of turbines causes a smaller reduction (MWF-WS: 12.08%). Although the MWF-Z0 case shows a stronger precipitation reduction than MWF inland (Figure 2.8), the percentage of precipitation reduction in the Houston area is lower than that of MWF (10.41% vs. 15.29%). The SWF case has the lowest precipitation reduction in all the cases (9.54%), which is possibly due to the absence of turbines in the Galveston Bay.

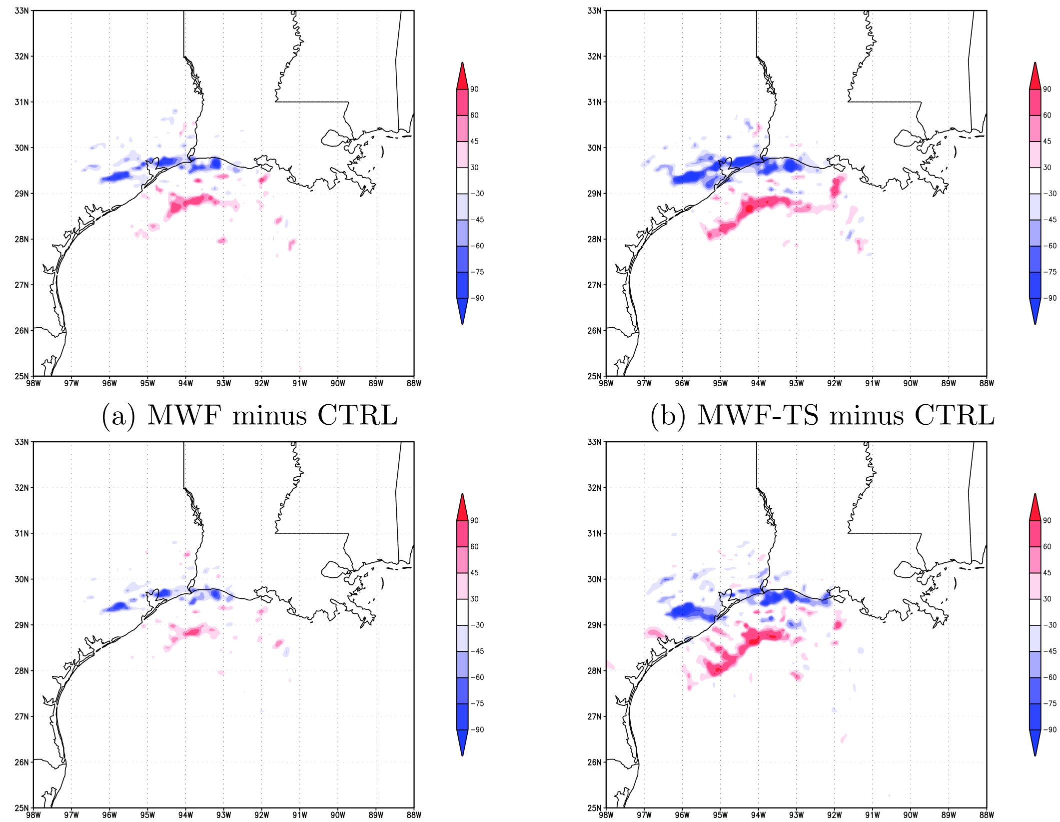

(a) MWF minus CTRL

(b) MWF-TS minus CTRL

(c) MWF-WS minus CTRL

(d) MWF-Z0 minus CTRL

Figure 2.8: 24-hour accumulated precipitation difference (mm) from 26 to 27 August 2017: a) MWF minus CTRL, b) MWF-TS minus CTRL c) MWF-WS minus CTRL d) MWF-Z0 minus CTRL.

Case ID	N. of turbines	Installed capacity (TW)	72-hour precipitation change in Houston (%)
CTRL	0	N/A	N/A
LWF	74,619	0.56	15.37
MWF	33,363	0.25	15.29
SWF	28,197	0.21	9.54
MWF-WS	22,242	0.17	12.08
MWF-TS	59,312	0.44	21.17
MWF-Z0	N/A	N/A	10.41

Table 2.3: Summary of the results for all the simulation cases.

2.4 Conclusions

The potential impacts of large arrays of offshore wind farms on precipitation during a hurricane are evaluated through the case study of Hurricane Harvey (2017) employing the the Weather Research Forecast (WRF) model. The simulations are setup without data assimilation and vortex initialization to isolate the potential effects induced by the wind farms, which would not be represented in the observations. The simulation without wind farms (control case) generally captures the life cycle of Harvey, but the maximum wind speed and precipitation are underestimated, while the minimum sea-level pressure is overestimated, in comparison with the observations. Overall, the simulation is considered to be adequate for the aims of this study.

A large array of offshore wind farms can have significant impacts on precipitation during hurricane. This claim is proven through a series of simulation cases, with different layout configurations, inter-turbine spacings, and wind-farm parameterizations. Precipitation is found to be reduced inland and increased offshore in all the wind turbine simulations. However, the amount of the reduction varies depending on the different cases. The location of the wind farm also matters and a larger wind farm may not necessarily induce correspondingly more reduction in precipitation. The wind turbines make a big difference only when the upstream wind is blowing from offshore to the land (upper-right side of the hurricane center in the northern hemisphere and for the Texas coast). The turbines on the other side of the hurricane center (i.e., lower-left) have a much weaker impact on precipitation. When the turbines are moved away from the coast, to respect a no-construction strip from the coast, the area with a significant reduction in precipitation also moves slightly offshore.

The alteration of precipitation patterns is caused by changes in horizontal wind divergence and in vertical velocity. Due to the reduced speed over the wind farm area, patterns of convergence upstream (offshore) and divergence downstream (inland) of the wind farms are formed, with consequent enhanced vertical motion upstream and reduced vertical motion downstream. As the turbines inhibit vertical upward movement of warm air downstream of the offshore wind farms (i.e., along the coast and even further inland), convection is partially offset and precipitation is therefore reduced. Vice versa, offshore and upstream of the wind farms, precipitation is enhanced. Although this study is focused on Hurricane Harvey, the mechanism proposed is expected to hold for any hurricane, although the exact impact on precipitation may vary with other hurricanes and coastlines.

Three different wind farm layouts, along with two inter-turbine spacings, are tested in the study. The MWF-WS case has the widest spacing and therefore the lowest number of turbines (22,242), which is still a futuristic number, considering that the largest offshore wind farm today (Anholt) includes 111 wind turbines. The aim of this study is to present this unexpected and potentially life-saving benefit, namely, the reduction of inland precipitation and flooding with offshore wind turbines. The next phase of this study will identify the smallest array size that still has significant benefits, focusing on the optimal layout that would maximize this benefit while, at the same time, minimizing the costs.

An important limitation of this study is that, with the current Fitch wind-farm parameterization, no sub-grid scale effects are considered. All the wind turbines within a grid cell are treated the same way, without considering their positions within the layout or the wind direction effects. As the number of wind turbines in the same grid cell ranges from 16 to 64, there can be significant wake effects and power losses within the grid cell for certain wind directions, which are neglected in the current study. A new wind-farm parameterization, which considers the wind turbine positions within the grid cell and is sensitive to wind direction (Pan and Archer, 2018), will be tested in the upcoming study on the optimal layout and size of offshore wind farms to reduce flooding and precipitation during hurricanes.

Chapter 3

A HYBRID WIND FARM PARAMETERIZATION FOR MESOSCALE AND CLIMATE MODELS

3.1 Introduction

Wind turbines extract kinetic energy from the atmosphere by means of their rotating blades, resulting in reduced wind speeds in the wake, which is the elevated plume-like volume downwind of wind turbines characterized by lower wind speeds and higher turbulent kinetic energy (TKE) than the upstream undisturbed flow. Because they cause a reduction in the power production of downwind turbines, wakes have been the subject of many studies based on observations (Dahlberg, 2009; Barthelmie et al., 2009, 2010; Chamorro and Porté-Agel, 2010; Hansen et al., 2012; Aitken et al., 2012; Iungo et al., 2013; Banta et al., 2015), numerical simulations (Ainslie, 1988; Larsen et al., 2007; Madsen et al., 2010; Calaf et al., 2010; Wu and Porté-Agel, 2011; Ott, 2011; Churchfield et al., 2012b; Brower and Robinson, 2012; Archer et al., 2013; Troldborg et al., 2014; Xie and Archer, 2015, 2017; Ghaisas et al., 2017), and analytical models (Jensen, 1983; Katic et al., 1986; Larsen, 1988; Frandsen et al., 2006; Bastankhah and Porté-Agel, 2014; Xie and Archer, 2015; Ghaisas and Archer, 2016).

Questions have been raised about if and how wind turbines and their wakes affect the lower boundary layer, especially the surface temperature, considering that the number of wind farms has grown rapidly in recent years as wind power has become the fastest growing renewable energy type (GWEC, 2014). Historically, these questions were first addressed with numerical simulations in two seminal papers published in 2004: Keith et al. (2004) at the global scale using a climate model, and Baidya Roy et al. (2004) at the regional scale using a mesoscale model. Since in both climate and mesoscale models the flow around the turbines cannot be fully resolved due to the coarse resolution (from hundreds of kilometres in climate models down to a few kilometres in mesoscale models), it has been necessary to develop an appropriate approach to represent the wind farms. Such an approach is called a wind farm parameterization because it represents the effect of the presence of the turbines without actually simulating all the details of the flow around them. For example, the wind farm parameterization presented in Keith et al. (2004) is simple, as the wind farm is represented as a region of increased surface roughness. Temperature values near the surface were found to both increase and decrease as a consequence of the presence of wind farms, without a consistent spatial or seasonal pattern. A few other studies followed, which similarly approximated turbines as either increased surface roughness or increased surface drag elements (Kirk-Davidoff and Keith, 2008; Barrie and Kirk-Davidoff, 2010; Wang and Prinn, 2010; Miller et al., 2011), but they have all been generally dismissed, because wind turbines do not extract energy near the surface but rather at hub height (80–100 m) and, therefore, their effects do not originate at the surface (Jacobson and Archer, 2012; Fitch et al., 2013b).

Baidya Roy et al. (2004) proposed a more advanced treatment of wind turbines as elevated sinks of momentum and sources of TKE. They ran a mesoscale model to simulate a large wind farm in which the turbines extracted kinetic energy with a constant power coefficient ($C_P = 0.40$), and the wakes were represented as cylinders with the same radius as the turbine blades, with a fixed amount of additional TKE per cylinder (5 m^2 s^{-2}). Many studies have since used the same principle of representing wind turbines as elevated momentum sinks, but proposed alternative methods and different grid sizes to calculate the extracted power, as well as the TKE of the wake. These include a power curve with no added TKE at the global scale (Jacobson and Archer, 2012), tabulated power and thrust coefficients with added TKE for regional applications (Fitch et al., 2012; Adams and Keith, 2013; Abkar and Porté-Agel, 2015), perfectly efficient turbines operating at the Betz limit globally with no added TKE (Marvel et al., 2013b), and a corrected power coefficient to account for mechanical and electrical losses in the turbines with the added TKE proportional to the extracted kinetic energy (Blahak et al., 2010). Two recent studies have accounted for the subgrid effects either by using wake-expansion equations (Volker et al., 2015) or by estimating the wake deflection (Vollmer et al., 2016).

Apart from the numerical simulations described above, a few field data and observations have also been used to evaluate the impacts of wind farms on the environment. Baidya Roy and Traiteur (2010) obtained data from a measurement campaign conducted in 1989 at the San Gorgonio wind farm (near Palm Springs in California), and found warming during the night and cooling during the day. However, the results of this measurement campaign are questionable because of the existence of aquifer-recharging ponds of water between rows of wind turbines, which likely had a stronger effect on the air temperature than the turbines themselves, but were not accounted for in the study (Archer et al., 2018). Using satellite data collected during days with clear skies, Zhou et al. (2012) found warming during the night and slight warming during the day over wind farms in Texas in contrast with nearby regions free of wind farms. Other studies (Smith et al., 2013; Rajewski et al., 2014; Armstrong et al., 2016) also found that the largest changes in temperature occur at night, whereas the changes in the daytime are not significant. Two field campaigns, the Crop Wind Energy Experiment (CWEX) in 2010 and 2011, took place in Iowa at a wind farm within crop fields. Cooling in unstable and warming in stable conditions was reported in the intermediate wake (at $\approx 17D$, where D is the rotor diameter), whereas weak warming was found near the surface in the far wake (at $\approx 35D$) for all atmospheric stabilities, and an inconsistent mix of warming and cooling in the near wake (Rajewski et al., 2013).

Consequently, no consistent conclusion has been made, and improved research is needed to resolve the inconsistencies between temperature effects and atmospheric stability. Since acquiring additional data via field campaigns has a high cost and may still lead to local and not general conclusions, improving the current wind farm parameterizations in which wind turbines are represented as elevated sinks of momentum and sources of TKE seems to be a logical and practical solution and, thus, is the proposed pathway here. Although these parameterizations are more advanced than those involving increased surface roughness or surface drag, they also have weaknesses, such as

1. the neglect of the wind direction, meaning that the effects of wind turbines in a grid cell on the surrounding environment (and on power production) are the same regardless of the wind direction;
2. the neglect of the wind farm layout, meaning that the position of the turbines within the grid cell is ignored, and all the turbines in the same grid cell are treated equally as "front-row" turbines, implying that the well-known and large wind speed and power reductions for turbines located in the second, third, and following rows of a wind farm are ignored within a grid cell;
3. the improper treatment of TKE generated by the wind turbines (either missing or excessive).

To explain the wind direction and layout effects, Fig. 3.1a shows two hypothetical wind farms with the same number of turbines (three), but with two different layouts. The two farms are treated as identical in existing wind farm parameterizations, even though they have obviously different responses to the wind direction. If the flow comes from the north, then the farm on the left has the largest wake losses because all turbines are aligned perfectly with the flow direction, but the farm on the right has no wake losses. In contrast, when the flow is from the west, the farm on the left is perfectly efficient, and the farm on the right has the worst wake losses.

Abkar and Porté-Agel (2015) attempted to resolve this problem by introducing a correction parameter ξ. While their results generally matched well with those from large-eddy simulations (LES), which are sophisticated, high-resolution, and computationally demanding simulations, the value of ξ was obtained by averaging over the LES results for which no predictive model or equation was provided. In other words, the LES runs have to be carried out first prior to every mesoscale simulation case with potentially different layouts and different wind directions. Thus, it is almost impossible to implement the correction proposed by Abkar and Porté-Agel (2015) due to its excessively high computational cost.

The ultimate effect of neglecting the wind direction and wind farm layout on the power production of the entire farm depends on the grid resolution, which influences

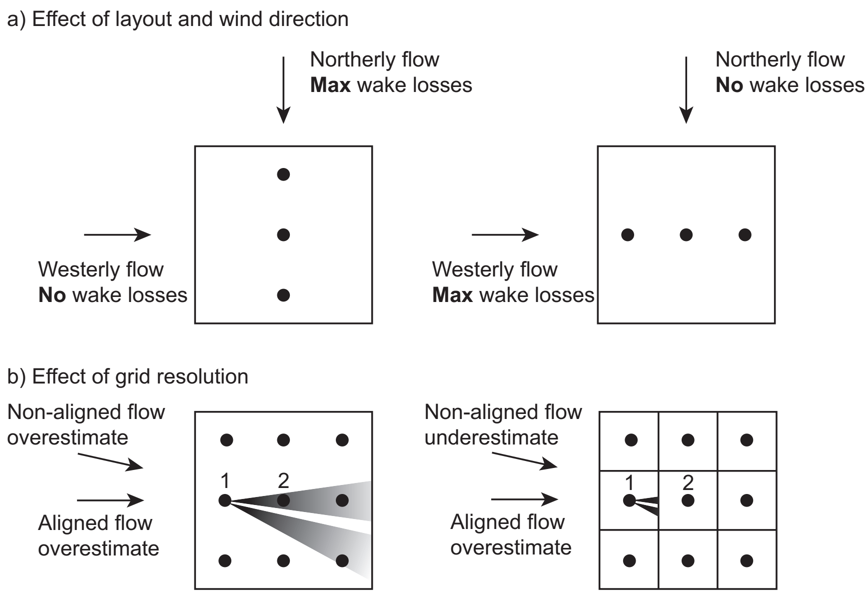

Figure 3.1: Schematic of the shortcomings of current wind farm parameterizations for (a) two wind farms having different layouts but (incorrectly) exactly the same wake losses for all cases, regardless of wind direction; and (b) based on turbines 1 and 2, where increasing the grid resolution from the farm on the left to that on the right causes turbine 2 to (incorrectly) produce excessive power for aligned wind directions, and too little power for non-aligned wind directions. The wakes are approximated as linearly expanding with triangular shapes in which the wind speed gradient is represented qualitatively by the shading from black (lowest speed) to white (highest speed). In the last farm, the wake effect of turbine 1 is only accounted for within its grid cell, and is represented by the small, black triangles.

the number of turbines per grid cell. Let us consider first the more common case in climate and mesoscale simulations where, due to the relatively coarse resolution (order of 10 km or more), the wind farm is entirely contained inside a single grid cell. In the real farm, every turbine encounters a different local upstream inflow depending on its position in the farm and the upstream wind direction. For example, in Fig. 3.1b in the left farm, the wake of turbine 1 in the front row affects the two turbines downstream when the flow is from the west. Therefore, turbine 2 generates much less power than turbine 1 in this case, but with regard to existing wind farm parameterizations, turbine 2 produces exactly as much power as turbine 1 because all the turbines in the grid cell are treated exactly the same as front-row turbines. Regardless of whether the wind direction is aligned or non-aligned with the rows and columns of the wind farm, at coarse resolution, the power production of the farm is overestimated because the subgrid-scale impacts of wakes are neglected.

At fine grid resolution (order of a few kilometres or less), the problem is more complicated, but, in general, an overestimation of power is still expected for wind directions that coincide with the directions of alignment of the rows and columns, and an underestimation for all other wind directions. As shown in Fig. 3.1b, the farm on the right is resolved with a fine resolution with one turbine per grid cell. When the flow is from the west, turbine 1 and 2 are aligned with the wind direction, and turbine 2 should generate significantly less power than turbine 1. However, the wind speed reduction caused by turbine 1 is distributed over the first grid cell by the wind farm parameterizations and, therefore, the resulting wind speed prior to turbine 2 is higher than in reality, and thus its power is overestimated. When the wind direction is non-aligned, however, turbine 2 should generate as much power as turbine 1, because it is not affected by the wake of turbine 1. Instead, the existing wind farm parameterizations still predict the same reduced, distributed wind speed as in the previous aligned case. As a result, the power generation of turbine 2 is underestimated.

These effects are confirmed by observations. Jiménez et al. (2015) simulated the Horns Rev wind farm with the Weather Research and Forecasting (WRF) model

(Skamarock et al., 2008) using the Fitch parameterization (Fitch et al., 2012) at high resolution (333 m). They find that the power is overestimated for the four directions of wind turbine–flow alignment (e.g., 0°, 90°, 180°, and 270°in their Fig. 3), and underestimated for all other directions, thus resulting in an unrealistically inefficient wind farm that "tends to overestimate the power deficit, except for the four directions with the highest deficits." At the Lillgrund wind farm, which is characterized by relatively tight spacing between turbines ($4.3D \times 3.3D$), Eriksson et al. (2015) used the same WRF-model set-up at 333-m resolution, and compared the power output with predictions made with an LES model and observations for a direction of alignment ($222^\circ \pm 2.5^\circ$). They found that the WRF model dramatically overestimates the power production (their Fig. 6).

To briefly summarize, if the spacing between turbines is large enough that the wake recovers prior to the next turbine, then wake losses are negligible, and parameterizations such as the Fitch variant are no longer affected by the turbine layout–wind direction shortcomings regardless of the grid resolution, because all the turbines behave as isolated ones and are effectively front-row turbines. No wind farm to date, however, has inter-turbine spacings sufficient enough to achieve negligible wake losses.

The third important aspect in a wind farm parameterization is to specify the correct amount of added TKE induced by the turbines. Jacobson and Archer (2012) formulated a wind farm parameterization for extracting kinetic energy and converting it to electricity based on the power curve of a commercial wind turbine. No additional turbulence from the turbine was added, so the resulting TKE in the grid cell was likely to be lower than the real value because it only included the effect of the resulting wind shear in the wakes. In the Fitch parameterization, a TKE-production term caused by the wind turbines was introduced, but has proven to overestimate values calculated from LES investigations by an order of 2–3 (Eriksson et al., 2015; Abkar and Porté-Agel, 2015). In another study, Vanderwende et al. (2016) used the Fitch parameterization in the WRF model, but disabled the TKE source term in the simulations, finding that some of the results are non-physical, with no advantages over the original formulation.

Volker et al. (2015) emphasized the importance of the vertical wake expansion of a single wind turbine, and derived an expression for the average subgrid turbine force, but they did not offer a method to estimate the added TKE.

All the weaknesses described above are ameliorated by the new hybrid wind farm parameterization presented here. A unique feature of the hybrid wind farm parameterization is that it takes advantage of knowledge gained via the sophisticated LES technique, making it possible to resolve the unsteady, turbulent flow around wind turbines, with high spatial and temporal resolutions (Pope, 2000). Starting around 2011, an increasingly large number of studies have utilized the LES approach to capture successfully the interactions between the wind farm and the atmosphere locally, at first under the simplified assumption of neutral stability (Calaf et al., 2010; Churchfield et al., 2012b; Wu and Porté-Agel, 2013; Archer et al., 2013; Xie and Archer, 2015), and then later under the more challenging unstable and stable conditions (Lu and Porté-Agel, 2011; Churchfield et al., 2012a; Mirocha et al., 2014, 2015; Aitken et al., 2014; Bhaganagar and Debnath, 2015; Wu and Porté-Agel, 2015; Lu and Porté-Agel, 2015; Creech et al., 2015; Ghaisas et al., 2017; Xie and Archer, 2017). Despite the high computational requirements of LES investigations, the effects on the local meteorology and surface temperature have been generally unclear because the LES duration is of the order of tens of minutes, which is too short to impact the thermal properties of the atmosphere, and because the relevant surface variables, such as temperature and the heat flux, are often prescribed and not predicted. However, the LES technique has been the most promising in terms of the simulation of flow dynamics and estimating power production and, therefore, it has been used extensively in our investigations. A suite of LES results described in Sect. 3.2 are used to calibrate the hybrid wind farm parameterization described in Sect. 3.3, with its applications within the mesoscale WRF model presented in Sect. 3.4, and validated against observations and additional LES data presented in Sect. 3.5.

3.2 The knowledge base: large-eddy simulations

Although LES investigations are computationally costly when studying large wind farms, the detailed LES data from several sets of investigations are invaluable in the development of a new wind farm model. The new hybrid parameterization is developed starting from the LES investigation of an existing wind farm, Lillgrund in Sweden, in which the local flow around each wind turbine is directly simulated at high spatial (≈ 3.5 m) and temporal (≈ 0.1 s) resolutions under neutral atmospheric stability following Archer et al. (2013).

3.2.1 Governing equations

The continuity, momentum (with the Coriolis force and Boussinesq approximation) and potential-temperature equations are

$$\frac{\partial \tilde{u}_i}{\partial x_i} = 0, \tag{3.1}$$

$$\frac{\partial \tilde{u}_i}{\partial t} + \tilde{u}_j \frac{\partial \tilde{u}_i}{\partial x_j} = -\frac{\partial \tilde{p}^*}{\partial x_i} - \frac{\partial \tau_{ij}^d}{\partial x_j} - \varepsilon_{ij3} f_c \tilde{u}_j + g\left(\frac{\tilde{\theta} - \theta_0}{\theta_0}\right)\delta_{i3} - f_i, \tag{3.2}$$

and

$$\frac{\partial \tilde{\theta}}{\partial t} + \frac{\partial \left(\tilde{u}_j \tilde{\theta}\right)}{\partial x_j} = \frac{\partial q_j}{\partial x_j}, \tag{3.3}$$

where i is 1, 2, or 3, the tilde denotes the LES filter of the velocity, pressure, and potential temperature, the modified pressure is defined as $\tilde{p}^* = \tilde{p}/\rho_0 + \tau_{kk}/3$, where $\tilde{p}$ is the filtered pressure, the deviatoric part of the subgrid-scale stress tensor is $\tau_{ij}^d = \tau_{ij} - \tau_{kk}\delta_{ij}/3$, where $\delta_{ij}$is the Kronecker delta, ε_{ijk} is the alternating unit tensor, and τ_{ij} is the kinetic stress tensor; the Coriolis parameter is f_c, $\tilde{\theta}$ is the resolved potential temperature, θ_0 is the reference temperature of 300 K, f_i is the body-force term (force per unit mass) induced by the turbine, and q_j represents the subgrid-scale heat flux. The summation convention over repeated indices applies. The unknown terms τ^d and q_j are computed with the eddy-viscosity and eddy-diffusivity methods, respectively (Smagorinsky, 1963). Since the hybrid wind farm parameterization is developed for much larger scales than those in the LES model, temporal and spatial (in the horizontal plane for each vertical level) averaging are required on the LES results, leading to

$$\frac{\partial\langle\overline{\tilde{u}_i}\rangle}{\partial t}+\langle\overline{\tilde{u}_j}\rangle\frac{\partial\langle\overline{\tilde{u}_i}\rangle}{\partial x_j}=-\frac{\partial\langle\overline{\tilde{p}^*}\rangle}{\partial x_i}+\frac{\partial\left(\langle\overline{\tau^d_{ij}}\rangle+\langle\overline{\tilde{u}_i''\tilde{u}_j''}\rangle\right)}{\partial x_j}+f_c\varepsilon_{ij3}\langle\overline{\tilde{u}_j}\rangle-\langle\overline{f_i}\rangle. \tag{3.4}$$

Here, the overbar and the bracket denote the temporal and spatial averages, respectively, $\tilde{u}_i''=\tilde{u}_i-\langle\overline{\tilde{u}_i}\rangle$, $\langle\overline{f_i}\rangle$ is the turbine induced force, which is modelled as a momentum sink in the new parameterization. In the LES model, $\langle\overline{f_i}\rangle$ can be obtained directly by application of spatial and temporal averaging of the body force f_i.

As shown by Abkar and Porté-Agel (2015), subtracting Eq. 3.4 from Eq. 3.2 and then multiplying it by $\tilde{u}_i''$, with the application of temporal and spatial averaging, the conservation equation can be written as

$$\begin{aligned}\frac{\partial\langle\overline{\tilde{e}}\rangle}{\partial t}=&-\langle\overline{\tilde{u}_j}\rangle\frac{\partial\langle\overline{\tilde{e}}\rangle}{\partial x_j}-\frac{\partial\langle\overline{\tilde{u}_j''\tilde{e}}\rangle}{\partial x_j}-\frac{\partial\langle\overline{\tilde{u}_j''\tilde{p}*''}\rangle}{\partial x_j}-\frac{\partial\langle\overline{\tilde{u}_j''\tau^{d\prime\prime}_{ij}}\rangle}{\partial x_j}\\&+\langle\overline{\tilde{u}_i''\tilde{u}_j''}\rangle\frac{\partial\langle\overline{\tilde{u}_i}\rangle}{\partial x_j}+\langle\overline{\tau^{d\prime\prime}_{ij}\tilde{S}_{ij}''}\rangle-\langle\overline{\tilde{u}_i''f_i''}\rangle,\end{aligned} \tag{3.5}$$

where $\langle\overline{\tilde{e}}\rangle$ is the spatially-averaged resolved TKE, $\tilde{S}_{ij}$ is the resolved strain tensor. In this TKE budget equation, only $\langle\overline{\tilde{u}_i''f_i''}\rangle$ is directly related to the turbine forces, and represents the added TKE produced by the wind turbines to be calculated via the new parameterization. To obtain this turbine-induced TKE production term P_{TKE} from the LES results, the relationship

$$\begin{aligned}\langle\overline{(\tilde{u}_i-\tilde{u}_i'')(f_i-f_i'')}\rangle&=\langle\overline{\tilde{u}_i}\rangle\langle\overline{f_i}\rangle\\&=\langle\overline{\tilde{u}_if_i}\rangle-\langle\overline{\tilde{u}_i''f_i''}\rangle,\end{aligned} \tag{3.6}$$

is used, so the turbine-induced TKE term P_{TKE} is obtained from

$$P_{TKE}=-\langle\overline{\tilde{u}_i''f_i''}\rangle=-(\langle\overline{\tilde{u}_if_i}\rangle-\langle\overline{\tilde{u}_i}\rangle\langle\overline{f_i}\rangle). \tag{3.7}$$

3.2.2 Large-eddy-simulation set-up and results

The Simulator for Offshore/onshore Wind Farm Applications (SOWFA), which was developed by the National Renewable Energy Laboratory based on the OpenFOAM toolbox (Churchfield et al., 2012a,b), is used to solve the Navier–Stokes equations (Eqs. 3.1–3.3). The discretization of the equations involves an unstructured, collocated, finite-volume framework, with pressure-implicit splitting for the time advancement of second-order accuracy in time. The turbine-induced forces f_i are computed using the actuator-line model (Shen and Sørensen, 2002), and projected to the flow field by

$$f_i = -\sum_{j=1}^{40} F_i^a \left(x_j, y_j, z_j, t\right)\right) \frac{1}{\varepsilon^3 \pi^{3/2}} \exp\left[-\left(\frac{|\vec{d_j}|}{\varepsilon}\right)^2\right], \tag{3.8}$$

where f_i is the body force in Eq. 3.2, F_i^a is the aerodynamic force at 40 equally spaced actuator points (x_j, y_j, z_j), ε is the projected width, and $\vec{d_j}$ is the distance from the blade point to each grid point. The effect of wind turbines is accounted for as an added body force f_i into the momentum Eq. 3.2.

The Lillgrund wind farm in Sweden, consisting of 48 wind turbines (Siemens 2.3 MW with diameter $D = 93$ m and hub height $H = 63.4$ m), was selected for simulation with the SOWFA model because of the tight turbine spacings $3.3D \times 4.4D$ and, therefore, high wake losses. Besides the original Lillgrund layout (Fig. 3.2a) with the prevailing wind direction of 225°(control case), a few additional LES investigations of two additional wind directions (270°and 315°) and a modified, staggered layout (Fig. 3.2b) were conducted, and used for the calibration of the hybrid parameterization. Details of the simulations are described in Archer et al. (2013). A summary of the LES cases considered here is listed in Table 3.1. Three additional wind farms with the same turbine type as Lillgrund, but with double spacing either in the along-wind, across-wind, or along- and across-wind directions were also simulated for the prevailing wind direction for validation purposes as discussed in Sect. 3.5.

The simulations are initiated with a so-called precursor run, which is carried out for 14,000 s with no wind turbines to generate a turbulent atmospheric boundary layer. The simulation with turbines starts after 12,000 s using the lateral boundary values

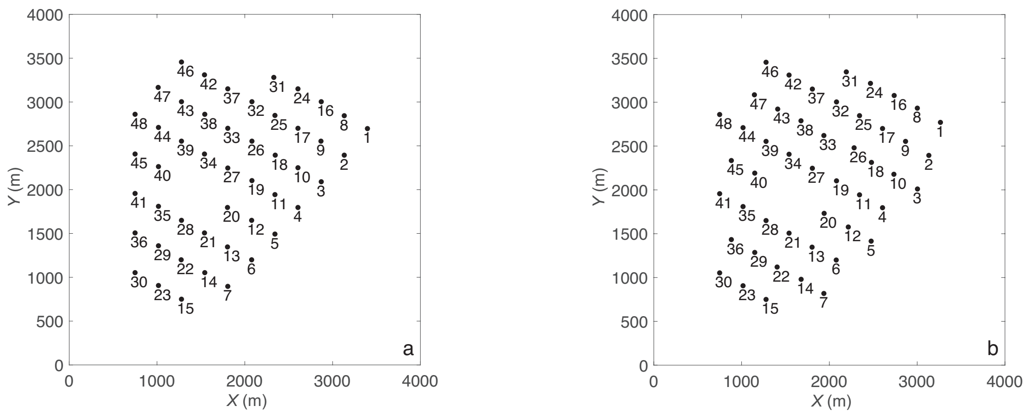

Figure 3.2: The Lillgrund wind farm in the computational domain for the (a) original and (b) staggered layouts.

saved from the precursor run for the time interval 12,000–14,000 s. The turbulence statistics, including for the velocity and body force, are processed starting from 12,200 s, and form the basis of the development and validation of the hybrid wind farm parameterization. The SOWFA model has been previously validated for its ability to simulate a precursor flow without turbines (Churchfield et al., 2012a), as well as the Lillgrund wind farm (Churchfield et al., 2012b). Some of the simulation results are shown in Fig. 3.3, where any turbine blocked or partially blocked by an upstream turbine clearly encounters a reduced upstream wind speed.

3.3 The hybrid wind farm parameterization: theoretical development

The theoretical development of the hybrid wind farm parameterization based on the LES results is introduced here.

3.3.1 Geometric properties and local upstream wind speed

In a mesoscale model, several turbines may fall into a single grid cell, so that the flow around each turbine is not resolved. As mentioned earlier, previous wind farm parameterizations are insensitive to the wind direction and turbine positions within the grid cell. To account for the effects of different wind directions and different farm

Case	Wind direction	Layout	Turbine number
225	225°	Original	48
270	270°	Original	48
315	315°	Original	48
225-STG	225°	Staggered	48
315-STG	315°	Staggered	48
225-L	225°	Double spacing along-wind	25
225-X	225°	Double spacing across-wind	23
225-LX	225°	Double spacing along-/across-wind	12

Table 3.1: Summary of the LES cases conducted to either calibrate the hybrid parameterization based on the original or staggered Lillgrund wind farm (top five cases) or to validate the hybrid parameterization at three wind farms with wider spacings in the along- and/or across-wind directions (bottom).

layouts, a parameterization based on a few geometric quantities is proposed. As the model is based partly on physical properties and partly on LES results, it is referred to as a "hybrid" model. This concept was first introduced by Ghaisas and Archer (2016), who used statistical models based on geometric quantities associated with the farm layout to predict the power of each turbine in a wind farm, as well as the average wind farm power output. The accuracy of the geometric model was validated against observations and LES results of the Lillgrund and Horns Rev wind farms. A similar approach is used to develop the hybrid model to predict the wind speed upstream of each individual turbine, and not just the power, based on the LES results presented above.

Given a wind farm layout and a wind direction, a few geometric quantities may be defined, with three of the five quantities described by Ghaisas and Archer (2016) used here. The first is the blockage ratio, which is defined as the fraction of the swept area of turbine n blocked by the swept area of any upstream turbine for a given wind direction. For each point (x, y) on the turbine rotor (e.g., 100×100 discrete points in

x and y) and for each wind direction θ, a discontinuous function λ is defined as

$$\lambda = \lambda(x, y, \theta) = \begin{cases} 1 & \text{if the point is blocked by any upstream turbine for wind direction } \theta, \\ 0 & \text{if the point is not blocked by any upstream turbine for wind direction } \theta. \end{cases} \tag{3.9}$$

The blockage ratio BR_n is the average value of λ at all the points within the turbine rotor disk area A, and can be written as

$$BR_n = BR_n(\theta) = \frac{1}{A} \iint_A \lambda \, dx \, dy. \tag{3.10}$$

The second quantity is the blockage distance BD_n defined as

$$BD_n = BD_n(\theta) = \frac{1}{A} \iint_A \left[\lambda L + (1 - \lambda) L_\infty\right] \, dx \, dy, \tag{3.11}$$

for each turbine n, where L is a function of the point (x, y) within the rotor disk, and denotes the distance to the nearest upstream blocking turbine. Here, L_∞ denotes the infinitely-large blockage distance when the grid point is not blocked by any upstream turbine ($\lambda = 0$); $L_\infty = 20D$ here since the recovery distance of the wake is about $20D$ according to previous studies (Porté-Agel et al., 2011; Xie and Archer, 2015).

The third quantity, which is the inverse blockage distance IBD_n, is a weighted average of the reciprocal of the blockage distances to upstream blocking turbines, weighted by the fraction of areas blocked

$$IBD_n = IBD_n(\theta) = \frac{1}{A} \iint_A \frac{1}{L} \lambda(x, y) \, dx \, dy. \tag{3.12}$$

Note that the blockage ratio, blockage distance, and inverse blockage distance are all a function of the wind direction.

The objective of the proposed hybrid model is to establish the relation between the wind speed upstream of each turbine, which is obtained from the LES results, and the three geometric quantities. The magnitude of the velocity V_n in front of each turbine n is normalized by the maximum wind speed V_{max}, which usually occurs at the front-row turbine, where "front-row" denotes the turbine that is not blocked by any upstream wind turbine in the layout. Although three geometric parameters are introduced, only the two with the highest correlation coefficients with the LES results, BR and IBD, have been used.

The hybrid model takes the general form of

$$\frac{V_n}{V_{max}} = h(BR_n, IBD_n), \tag{3.13}$$

where h is a multiple linear regression function whose coefficients are calibrated based on the $5 \times 48 = 240 V_n$ values from the five LES runs. The wind turbines with $BR = 0$ are considered to be the front-row turbines subject to the undisturbed flow. To improve the accuracy of the model, the front-row wind turbines are excluded from the linear regression, and the fitting coefficients

$$h(BR_n, IBD_n) = \begin{cases} 0.9615 - 0.1549 BR_n - 0.0114 IBD_n L_\infty & BR_n \neq 0 \\ 1 & BR_n = 0 \end{cases} \tag{3.14}$$

are obtained. Note again that all variables in Eq. 3.14 depend on θ. To measure the strength of the linear correlations between the relative velocity V/V_{max} from the LES results (X) and from the hybrid model (Y), the linear correlation coefficient

$$\rho(X,Y) = \frac{E[XY] - E[X]E[Y]}{\sqrt{E[X^2] - E[X]^2}\sqrt{E[Y^2] - E[Y]^2}} \tag{3.15}$$

is used, where E is the ensemble average. Despite its simplicity, the hybrid model works remarkably well, with $\rho = 0.9335$. Figure 3.4 compares the upstream wind speed predicted with the hybrid model h versus the raw LES data from the five simulations (denoted with different markers). The proposed linear fit is a good approximation for the normalized upstream wind speed. Note that wake meandering (España et al., 2011), which is the subgrid-scale, semi-random oscillation of the wake around its main axis, is indirectly accounted for in the fitting coefficients of the hybrid model, because the LES results on which it was based correctly capture wake meandering.

3.3.2 Momentum extraction and added turbulent kinetic energy

The Fitch wind farm parameterization (Fitch et al., 2012), which has been implemented into the WRF model, is the most widely used method to simulate large wind farms. Because some of the terms and approximations used in the Fitch parameterization have been adopted, the Fitch equations are introduced here, followed by the new proposed equations for the hybrid parameterization, which also includes some concepts from Abkar and Porté-Agel (2015). The results with both models (Fitch and hybrid as stand-alone off-line models not yet inserted into the WRF model) at the Lillgrund wind farm are presented below.

The drag force on the atmosphere induced by the turbines can be expressed as an elevated drag

$$F = \frac{1}{2} C_T(V) \rho V^2 A, \tag{3.16}$$

where V is the horizontal wind speed over the rotor disk, C_T is the thrust coefficient, ρ is the air density, and A is the rotor area. The power available in the flow P_A is, therefore,

$$P_A = \frac{1}{2} C_T(V) \rho V^3 A, \tag{3.17}$$

which consists of two parts (mechanical losses are not considered) as proposed originally by Adams and Keith (2007).

1. The electric power P_E, which is given by

   $$P_E = \frac{1}{2} C_P(V) \rho V^3 A, \tag{3.18}$$

   where C_P is the power coefficient of the turbine; and

2. the power lost to the flow in the form of additional TKE, which can be expressed by the turbine-induced TKE term (an added-TKE term)

   $$P_{TKE} = \frac{1}{2} C_{TKE}(V) \rho V^3 A, \tag{3.19}$$

   where $C_{TKE} = C_T - C_P$.

Physically, this means that not all the energy extracted (via C_T) can be converted to electricity (via C_P) because some is converted to turbulence instead (via C_{TKE}). Fitch et al. (2012) improved this model by assuming that each wind turbine occupies multiple vertical atmospheric layers, rather than one layer, and coupled it with the WRF model. Considering the Cartesian coordinate system with grid indices i, j, k, corresponding to the x, y, z directions, the momentum-tendency term at each grid point (i, j, k) can be written as

$$\frac{\partial V_{ijk}}{\partial t} = -\frac{\frac{1}{2} N_{ij} C_T(V_H) V_{ijk}^2 A_{ijk}}{\Delta x \Delta y (z_{k+1} - z_k)}, \tag{3.20}$$

where N_{ij} is the number of wind turbines in the grid column (i, j), and V_H is the wind speed at hub height. Note that neither the effects of wind farm layout nor wind direction are included in Eq. 3.20, since the same grid-cell velocity V_{ijk} is used for all the turbines in the same grid cell, regardless of their position or wind direction. The added TKE term in a grid cell $P_{T,ijk}$ is modelled as

$$P_{TKE,ijk} = \frac{\frac{1}{2} N_{ij} C_{TKE}(V_H) V_{ijk}^3 A_{ijk}}{\Delta x \Delta y (z_{k+1} - z_k)}. \tag{3.21}$$

In all previous parameterizations, including Fitch's, both the turbine location within a grid cell and the wind direction make no difference in estimating the extracted momentum, which means that two different layouts with the same number of turbines in a grid cell give the exact same effect in the mesoscale model with regard to the extracted power, added TKE, and the mean flow properties. As such a parameterization has the same effect for all wind directions, this implies all turbines are treated as front-row turbines, regardless of their actual position or the actual wind direction, which is obviously a shortcoming. Not surprisingly, Eriksson et al. (2015) performed simulations of Lillgrund using both LES and WRF models, and found large discrepancies (overestimates in that case) between the power predicted with the WRF model and that by both LES results and actual observations.

To solve this issue, we modified Eq. 3.20 by introducing the hybrid model developed in Eq. 3.14. Instead of using the same velocity V_{ijk} for all the turbines in a grid cell, the turbines are treated individually. For each individual wind turbine n, the upstream velocity is corrected with the function h, which depends on both the location of the turbine n and the wind direction,

$$V_{n,ijk} = h(BR_n, IBD_n)V_{ijk}, \tag{3.22}$$

where $h(BR_n, IBD_n)$ is the fitted function based on the blockage ratio and inverse blockage distance. Therefore, only the front-row turbines are subject to the velocity V_{ijk} and, thus, $h = 1$. Since BR and IBD both depend on the wind direction, the function $h(BR_n, IBD_n)$ is also a function of the wind direction. Although $h(BR_n, IBD_n)$ was originally developed based on the average velocity over the disk area, here it is assumed that $h(BR_n, IBD_n)$ applies to every vertical level within the rotor disk area.

The magnitude of the momentum-tendency term of each grid cell (i, j, k) can now be written as

$$\langle \overline{f} \rangle = |\frac{\partial V_{ijk}}{\partial t}| = \sum_{n=1}^{N^{ij}} \frac{\frac{1}{2}C_T(V_H)V_{ijk}^2 h^2(BR_n, IBD_n)A_{ijk}}{\Delta x \Delta y(z_{k+1} - z_k)}. \tag{3.23}$$

The other important term to be modelled is the turbine-induced added TKE (P_{TKE}), which does not include the contribution from the increased vertical shear resulting from the momentum sink, but only the contribution from the velocity fluctuations caused by the turbine-induced forces ($\langle \overline{\tilde{u}_i'' f_i''} \rangle$ in Eq. 3.5). Instead of assuming that the turbines inside a grid cell behave similarly and have the same performance, each individual turbine here is treated separately, as done previously for the normalized upstream wind speeds.

In Abkar and Porté-Agel (2015)'s solution, the added-TKE term is written as

$$P_{TKE} = -\langle \overline{\tilde{u}_i'' f_i''} \rangle = \langle \bar{f}_i \rangle \left(\langle \overline{\tilde{u}_i} \rangle - \overline{\tilde{u}_d} \right), \tag{3.24}$$

where $\langle \overline{\tilde{u}_i} \rangle$ is the temporal and spatial average of velocity for each vertical level of the LES domain, and $\overline{\tilde{u}_d}$ is the temporal-average velocity at the turbine disk. The disk velocity $\tilde{u}_d$ is defined as

$$\tilde{u}_d = U_\infty(1 - a) = U_\infty(1 - 0.5(1 - \sqrt{1 - C_T})), \tag{3.25}$$

where U_∞ is the undisturbed upstream velocity, and a is the induction factor

$$a = 0.5(1 - \sqrt{1 - C_T}). \tag{3.26}$$

Since the undisturbed upstream velocity U_∞ is not directly available from the mesoscale model, the spatial-averaged velocity at hub height from the LES output, which corresponds to the velocity at the hub-height level in the mesoscale model, are used to approximate the upstream velocity in Eq. 3.25 as

$$\overline{\tilde{u}_d} = \langle \overline{\tilde{u}_i} \rangle (1 - 0.5(1 - \sqrt{1 - C_T})). \tag{3.27}$$

For each grid cell at every vertical level, replacing the domain-averaged speed $\langle \overline{\tilde{u}_i} \rangle$ in the LES model with the mesoscale grid-cell speed V_{ijk}, the turbine-induced $P_{TKE,ijk}$ can be written as

$$P_{TKE,ijk} = \sum_{n=1}^{N^{ij}} \frac{\frac{1}{2} C_T(V_H) V_{ijk}^3 h^2(BR_n, IBD_n) 0.5(1 - \sqrt{1 - C_T}) A_{ijk}}{\Delta x \Delta y (z_{k+1} - z_k)}. \tag{3.28}$$

The resulting forces and TKE-production term derived above are compared with both the LES and Fitch-model results in Figs. 3.5 and 3.6, respectively. Note that neither the Fitch nor the hybrid model have yet been coupled with the WRF model. Instead, the two models have been run off-line using the LES domain-averaged velocities spanning the vertical levels as inputs. The purpose of the comparison is to prove that, at least for Lillgrund, the performance of the hybrid model is satisfactory, thus providing confidence for coupling with the WRF model. The modelled turbine-induced force and added-TKE term generally agree very well with the LES results. The Fitch model overestimates $\langle \overline{f} \rangle$ and, thus, overestimates the energy extracted from the atmosphere (Fig. 3.5), which is consistent with Eriksson et al. (2015) for Lillgrund and with Jiménez et al. (2015) for Horns Rev along the alignment directions.

Since the Fitch model does not include any wake effects within a single grid cell, the wake losses are neglected within the grid cell, and the power is overestimated. Actually, if the value of $h(BR_n, IBD_n)$ in the turbine-induced force Eq. 3.23 is set to one (i.e., the turbines become front-row turbines), then the result will be exactly the same as with the Fitch model, which supports our interpretation that Fitch treats all turbines as front-row turbines. In addition, the added-TKE term is overestimated by a factor of 2–3 by the Fitch model (Fig. 3.6). Note that the added -TKE term here is directly related to the turbine forces and does not include the contribution of vertical wind shear. Because the hybrid model is capable of reproducing the LES effects when given the right inputs, it may be coupled with the planetary-boundary-layer parameterization in the WRF model, as presented in the next section.

3.4 The hybrid wind farm parameterization: application in the Weather Research and Forecasting model

The theoretical foundation for the new wind farm parameterization was presented in the previous section. In this section, the results of the hybrid parameterization within the WRF model for idealized simulations of the Lillgrund wind farm are analyzed and compared with LES results and observations.

3.4.1 Implementation of the hybrid parameterization in the Weather Research and Forecasting model

The hybrid wind farm parameterization presented above is implemented into the planetary-boundary-layer parameterization in the WRF model by imposing a momentum sink and adding a TKE source term for which the Mellor–Yamada–Nakanishi–Niino (MYNN) model (Nakanishi and Niino, 2009) is chosen, as done in previous studies (Fitch et al., 2012; Volker et al., 2015). The MYNN model is based on the Mellor–Yamada turbulence closure model (Mellor and Yamada, 1974, 1982), with the effects of buoyancy on pressure covariances and stability on the turbulence length scale included. As the MYNN model determines the empirical closure constants from another LES database of the dry atmosphere, the prediction of TKE is more reliable.

The MYNN model is a 2.5-level, 1.5-order parameterization, with only one prognostic equation for the second-order moments, i.e., the TKE,

$$\frac{\partial e}{\partial t} = T + P_s + P_b + P_{TKE} - \epsilon, \tag{3.29}$$

where $e = q^2/2$ denotes the TKE per unit mass and $q^2 = 2e$, with other high-order terms determined diagnostically. Here, T combines the turbulence transport of TKE and the pressure distribution term, and is modelled using eddy diffusion by

$$T = -\frac{\partial}{\partial z}\left(\overline{w'e} + \frac{1}{\rho}\overline{w'p'}\right) = \ell q S_q \frac{\partial}{\partial z}(\frac{q^2}{2}), \tag{3.30}$$

where P_s is the turbulence production from the vertical shear in the horizontal velocity, and P_b is the buoyancy-production term

$$P_s = -(\overline{u'w'}\frac{\partial \bar{u}}{\partial z} + \overline{v'w'}\frac{\partial \bar{v}}{\partial z}), \tag{3.31}$$

$$P_b = \frac{g}{\bar{\theta}_0}\overline{w'\theta'}, \tag{3.32}$$

respectively.

The second-order turbulence-flux terms $\overline{u'w'}, \overline{v'w'}$ and $\overline{w'\theta'}$ can be expressed in terms of vertical gradients as

$$\overline{u'w'} = -\ell q S_M \frac{\partial \bar{u}}{\partial z}, \tag{3.33}$$

$$\overline{v'w'} = -\ell q S_M \frac{\partial \bar{v}}{\partial z}, \tag{3.34}$$

and

$$\overline{w'\theta'} = -\ell q S_H \frac{\partial \bar{\theta}}{\partial z}. \tag{3.35}$$

The term P_{TKE} is the turbulence induced by the wind turbine given by Eq. 3.28, and ϵ is the rate of dissipation of TKE expressed as

$$\epsilon = \frac{q^3}{B_1 \ell}. \tag{3.36}$$

Equations 3.30 to 3.36, u', v and w' are the turbulent components of the velocity vector, the overline denotes an ensemble average, θ' is the turbulent component of potential temperature, θ_0 is the reference potential temperature, p is the air pressure, ρ is the air density, g is the acceleration due to gravity, B_1 is a closure constant, ℓ is the mixing length, and S_q, S_M, S_H are the stability functions for q, momentum and heat, respectively. With all the terms above modelled, the prognostic equation for TKE (Eq. 3.29) can be integrated in time. The eddy diffusion K_M is then given by

$$K_M = \ell q S_M. \tag{3.37}$$

The WRF model coupled with the hybrid wind farm parameterization is referred to as the "WRF–hybrid" model, with the standard coupling with the Fitch parameterization labelled as the "WRF–Fitch" model.

3.4.2 Weather Research and Forecasting model configuration

Idealized simulations of the Lillgrund wind farm are carried out with version 3.6 of the WRF model to facilitate the comparison of the results with the LES data. The wind farm is placed at the centre of a 160×160 km domain to minimize the interference from the boundaries of the domain, which has a horizontal resolution of 4×4 km. All 48 turbines are placed within one grid cell, which is the size of the whole LES domain, to ensure a fair comparison with the LES domain-averaged properties. In There are 44 vertical levels with a higher resolution in the lower boundary layer (200 m). The vertical resolution below 200 m is 7.5 m in the first two levels, 10 m in or near the grid cells that intersect with the turbine blades, and ranges from 15 m to 25 m above the rotor. The surface flux and radiation schemes are turned off to isolate the turbulence mixing induced by the wind farm. Open lateral boundary conditions are applied at all the lateral boundaries. The bottom surface is modelled as a water surface of roughness 0.016 m (consistent with the LES set-up), with application of the no-slip condition. At the top, the Rayleigh relaxation layer is used to control the reflection of waves. The simulations are initialized with a mean velocity profile that follows the logarithmic law

$$U(z) = \frac{u_*}{\kappa} \ln \frac{z}{z_0}, \tag{3.38}$$

where u_* is the friction velocity, κ is the von Karman constant, and z_0 is the surface roughness length mentioned above ($z_0 = 0.016$ m).

Three wind directions $(225°, 315°, 270°)$ corresponding to the LES simulations in Table 3.1 are modelled with both our hybrid parameterization and the Fitch parameterization. The flow is driven by a horizontal pressure gradient to a constant geostrophic wind speed at $z = 90$ m, consistent with the LES set-up. To achieve the same preconditions as in the LES results without wind farms, the WRF simulations for the three wind directions are initialized with uniform geostrophic wind speed components (u along x and v along y) as

- 225°: $u = 10.5$ m s^{-1}, $v = 5.4$ m s^{-1};
- 270°: $u = 11.4$ m s^{-1}, $v = -3.8$ m s^{-1};
- 315°: $u = 5.4$ m s^{-1}, $v = -10.7$ m s^{-1}.

Next, the WRF runs without the turbines are integrated for three days, achieving a steady neutral boundary layer in good agreement with that simulated with the precursor LES set-up. The wind farm parameterization is then activated, and the simulations restarted from the steady boundary layer described above.

3.4.3 Results of the Hybrid and Fitch parameterizations

The WRF simulations with the wind farm are carried out for another 6 h to achieve a steady state. The data from the grid cell that contains the wind farm are compared with the LES data after a temporal and spatial average is calculated over the entire LES domain.

From the vertical profiles of wind speed (Fig. 3.7), the WRF model is in excellent agreement with the LES model at the precursor stage (i.e., without the wind farm).

In the presence of the wind farm, the wind speed profile predicted by the WRF–hybrid model agrees very well with the LES results, and is generally better than the WRF–Fitch model, which overestimates the wind speed deficit over the entire rotor area, particularly at hub height, by approximately 0.4 m s^{-1}. The overestimate is larger when the turbines are aligned with the wind direction with tight spacing (see the 225° case in Fig. 3.7a, where the spacing is $4.3D$) and smaller when the wind direction is either non-aligned (see the 315° case in Fig. 3.7b) or the spacing between turbines is large (see the 270° case in Fig. 3.7c, where the spacing is $8.5D$). Note that an overestimation of the wind speed deficit leads to an overestimation of the power extraction by the turbines and, hence, the power production of the wind farm. A common weakness of both hybrid and Fitch models is that the wake has a lower vertical extent than that suggested by the LES simulations as shown by the excessive recovery of the deficit of both models above the upper tip of the blades.

The vertical distribution of TKE shown in Fig. 3.8 again confirms the good performance of the WRF–hybrid model compared with the WRF–Fitch model, which overestimates TKE by about 50% at hub height for all directions. Both models correctly produce a peak in TKE above hub height, but at a height 10–20 m below that simulated by the LES model, which is consistent with the lower vertical extent of the wake mentioned above. Note that the TKE near the ground simulated by the WRF model differs from that simulated by the LES model, regardless of the wind farm parameterization, due to the insufficient vertical resolution of the WRF model near the ground, and the different methods used in modelling the lower boundary condition.

In summary, the hybrid parameterization was successfully implemented in the WRF model, with the results for three cases (with three different wind directions) at Lillgrund comparing well with the LES results in terms of the wind speed and TKE profiles over the entire wind farm. Although this good agreement was expected, since the hybrid model was calibrated with five LES cases, including the three cases simulated with WRF model, it was important to prove that the hybrid parameterization, when inserted in the WRF model (WRF–hybrid model), reproduces the LES results accurately and generally better than the current wind farm parameterization available in the WRF model.

3.5 Validation

Although the power production of the wind farm is not required for developing and running the parameterizations, the power of each wind turbine is considered here to further verify the accuracy of the hybrid model, since power data are easier to collect than velocity or TKE data. A proprietary dataset of actual power production at Lillgrund for about 16 months at a time resolution of 1 min or less was provided by Vattenfall. The dataset was quality-checked, with errors, such as the yaw bias or excessive pitch angles, removed for wind directions approximating perfect alignment with the turbine columns because the maximum local wake deficit must occur for those directions and, therefore, the yaw bias can be determined as described in Ghaisas et al. (2017). Not all the turbines could be corrected for all wind directions because, identifying a truly undisturbed front-row turbine was not always possible, while not all columns had a sufficient number of turbines. For example, for the south-westerly direction (225°), only the columns led by turbines 15, 23 and 30 (Fig. 3.2a) were quality-controlled because of the shorter lengths of the columns led by other turbines, e.g., 7 or 36, or the front-row turbine is partially affected by nearby turbines.

In the hybrid model, the wind speed upstream of each individual wind turbine at hub height is calculated directly and, therefore, the power output of each turbine can be obtained from the power curve (with linear interpolation between the discrete values of wind speed published by the manufacturers). The power is then normalized by the power of the front-row turbine, which is referred to as the relative power. Note that the relative power of all turbines according to the Fitch parameterization is one because they are all treated as front-row turbines.

To verify the WRF–hybrid and WRF–Fitch models, the LES results, the original geometric model results from Ghaisas and Archer (2016), and the observations from the Vattenfall dataset (if available) are compared in Fig. 3.9. The relative power from the

	225°	315°	270°
LES	0.619	0.806	0.691
Geometric model	0.625	0.789	0.697
Hybrid	0.636	0.782	0.700
Fitch	1	1	1

Table 3.2: Summary of wind farm average relative power at Lillgrund for three wind directions from the WRF–hybrid and WRF–Fitch models, the geometric model of Ghaisas and Archer (2016) and LES results.

hybrid model generally matches the LES and geometric model results remarkably well for all three directions, as expected given that the hybrid model is calibrated based on the LES data. The hybrid model also performs well compared with the observations, especially for the two directions 315° and 270°. The Fitch model always overestimates the power output of turbines not in the front row, regardless of the wind direction, and by as much as a factor of two (e.g., for 315°, the relative power of turbine 11 is about 0.5, but the Fitch model predicts a relative power of one). The performance of all models for the 225° direction is worse than along the other directions, with the predicted relative power often lying outside of one standard deviation around the mean of the observations (Fig. 3.9a). A possible explanation is that the turbines are actually aligned along 221.6°, and not 225°. Also, the observations reflect a variety of wind speeds, atmospheric stability conditions, and turbulence intensities not captured in any of the model runs.

An interesting case is that of turbine number 11 for the 270° wind direction (Fig. 3.9c), where the only turbine upstream of turbine 11 is turbine 41 (Fig. 3.2a) because of the "hole" void of turbines in the middle of Lillgrund. The distance between the two turbines is around $18D$, and the LES results indicate that the wake of turbine 41 has almost dissipated before reaching turbine 11 and, therefore, the relative power of turbine 11 is high (0.9). However, in both the geometric and the hybrid models, turbine 11 is still considered blocked because the blockage distance is within the maximum $L_\infty = 20D$. Sensitivity tests to find the optimal value of L_∞ will be conducted to improve this in a future study.

In all previous wind farm parameterizations, all the turbines in the same grid cell are treated as front-row turbines and, thus, the total power output of the wind farm is overestimated if the farm is contained in a single grid cell, such as for these simulations. To get a sense of the magnitude of this overestimate, the wind farm average relative power from the different methods in the three wind directions are listed in Table 3.2. The hybrid model is very close to both the LES and the geometric model results, while the Fitch parameterization (and possibly all previous parameterizations) overestimates the power by 61.6% (225°), 24% (315°), 44.8% (270°). Again, the WRF–Fitch model performs better for the non-aligned wind direction of 315° because more turbines are exposed to the undisturbed flow when the wind direction is not from a direction of alignment and, therefore, more turbines effectively behave like front-row turbines in such cases.

The hybrid parameterization was calibrated with the five LES cases described in Sect. 3.2, with three based on Lillgrund, including two for a staggered version of Lillgrund. However, Lillgrund is a tightly-spaced wind farm with large wake losses and is, therefore, possibly the most challenging case to simulate correctly with a wind farm parameterization. To prove that the hybrid model also works with other wind farms, especially less tightly-spaced layouts, three additional wind farms were simulated with both LES and WRF models for the same south-westerly wind direction. Compared with the original Lillgrund layout, the three new farms are characterized by double spacing in the along-wind (case 225-L in Table 3.1), across-wind (225-X), and both along- and across-wind (225-LX) directions. The details of the LES set-up of the three new wind farms, referred to as the double-spaced cases, are described in Archer et al. (2013) and the layouts are shown in Fig. 3.10.

The relative power and the velocity profiles at the three double-spaced wind farms simulated with the WRF–hybrid model are compared with those from the LES and WRF–Fitch models in Fig. 3.11. A similarly remarkable agreement is reached between the LES results and the hybrid-parameterization results for the relative power, not only in terms of the wind farm average power, but also for each turbine. As expected, the wind farm with the tightest along-wind spacing, i.e., 225-X with $4.3D$, is the least efficient (relative power $\approx$ 0.6), and is only marginally better than the original Lillgrund layout for 225°(Fig. 3.9a), suggesting that increasing the across-wind spacing is ineffective at reducing wake losses. The two layouts with the largest along-wind spacing, i.e., 225-L and 225-LX, are both more efficient than the original, with a relative power around 0.8. The vertical wind speed distribution is also found to agree well with LES results for all three double-spaced cases. While the Fitch parameterization still overestimates the wind speed deficit in all the three cases, the overestimate is much smaller in the 225-LX case.

3.6 Sensitivity to multi-grid wind farm modeling

While the hybrid parameterization has been validated and proven to be an accurate tool to model the effects of wind farms in a mesoscale model, all the simulations so far were run with all the turbines placed in a single grid cell. As large wind farms, however, are likely to occupy multiple grid cells of a mesoscale model, the hybrid model needs to be adapted to properly incorporate spatial variations of wind direction and wind speed within such large multi-grid farms.

Two methods are proposed here to model a wind farm that occupies multiple grid cells. The first method is similar to the case where all the turbines are in a single grid cell, where the geometric properties of each turbine are calculated considering the wind turbines all together as a whole. All the wind turbines share the same upstream velocity, but the momentum sink and the added-TKE terms are applied to each grid cell occupied by the turbines. To determine the wind direction and the front-row turbine at each time step, the wind directions of the grid cells containing the turbines are calculated, and then the average wind direction is used to further evaluate the geometric properties and the front-row turbine. The first method is only valid for medium-sized wind farms without strong spatial variations of wind direction and wind speed. Because of its limited applicability, the first method is not recommended as a general solution to the multi-grid problem. It is included here because it is simple to apply and it helps in the evaluation of the sensitivity of the hybrid model to the grid cell treatment.

To account for significant spatial variations of wind direction and wind speed within large wind farms, a second method is proposed, which considers the wind turbines in the wind farm locally and individually. When calculating the geometric properties of a wind turbine, not all the upstream turbines are considered. Only the wind turbines within a certain maximum effective distance from the current wind turbine (ED) are considered. The maximum ED is 17.5D in this study and the reason is discussed later. For example, for the north-westerly direction (315°), turbine 6 may be blocked by turbines 40 and 48 (shown in Fig 3.12 b), but only turbine 40 will be considered since turbine 48 is more than $17.5D$ away. With this setup, a local wind farm, with turbine 40 as the new front-row turbine, is constructed to evaluate the turbine-induced forces and added-TKE term. For turbines in different grid cells, the local wind speed and wind direction are used, and, thus, the effects of the variations of wind direction and wind speed in large wind farms are included.

For the first method, a 9 grid-cell case is tested, denoted as 9CELL-MT1. For the second method, a more complicated 16 grid-cell case is tested, denoted as 16CELL-MT2. For both the cases, two wind directions are evaluated.

From Fig. 3.13, both multigrid methods with the hybrid parameterization slightly overestimate the wind-speed deficit, but are still more accurate than the Fitch parameterization. The relative power (Fig. 3.14) obtained from 9CELL-MT1 is slightly larger than the results obtained from the case with all the turbines in one grid cell (1CELL), but the error is within 5%. Also, the 16CELL-MT2 case is in better agreement with LES than any other case. As the wind-farm average relative power is closer (dash lines in the figure) compared to other models (see Table 3.2).

To estimate the value of the maximum effective distance, a few test cases with different values were run and the wind-farm average powers are summarized in Table 3.3. For both wind directions, the wind-farm average power is relatively steady when

	15.5D	16.5D	17.5D	18.5D	19.5D	LES
225°	0.628	0.627	0.624	0.624	0.610	0.619
315°	0.812	0.805	0.805	0.804	0.785	0.806

Table 3.3: Summary of wind-farm average relative power at Lillgrund for two wind directions using five possible effective distances and LES results.

the maximum effective distance between 17.5D and 18.5D and is also close to LES results, so the maximum ED is likely within this range.

3.7 Conclusions and future work

To model the effects of a wind farm on weather and climate systems, a new hybrid wind farm parameterization is proposed here for mesoscale and climate models. In contrast to previous wind farm parameterizations that treat all wind turbines occupying the same grid cell as front-row turbines regardless of both their actual position within the wind farm and the wind direction, the new hybrid parameterization eliminates these two weaknesses by including the effects of both wind farm layout and wind direction via a statistical model calibrated with the results of high-resolution LES cases.

The hybrid model is based on a few geometric properties, namely the blockage ratio and inverse blockage distance, which are directly connected to the relative locations of the turbines in the layout for each wind direction. The model predicts the wind speed upstream of each individual wind turbine with a high correlation with the LES results (> 0.93). The turbines are modelled as elevated momentum sinks and TKE sources derived analytically as a function of the predicted upwind wind speed, and are implemented in the WRF model. The results show that the hybrid wind farm parameterization performs well in terms of both the predicted vertical profiles of relevant physical properties, such as the wind speed and TKE, and the power production. Comparisons with LES results and with observations at the Lillgrund wind farm indicate that the hybrid model improves upon the existing wind farm parameterization in the WRF model, with lower turbulence in the wakes and lower power production.

To verify the hybrid parameterization for wind farms other than Lillgrund, three hypothetical wind farms with larger spacings for along- and/or across-wind directions have been modelled and compared with the LES results, with similarly good agreement achieved for both power and wind speed predictions. Although the model is calibrated based on a few cases of the original and staggered Lillgrund wind farm, the hybrid parameterization accommodates other configurations and other wind farm layouts, regardless of the particular spacing.

While the hybrid wind farm parameterization is a promising tool to replicate the effect of wind farms on the surroundings, more work is needed on the following two aspects. First, the geometric properties have been calibrated based on LES results obtained under neutral conditions and, therefore, are insensitive to atmospheric stability, which has been shown to have an important effect on wind farm production (Magnusson and Smedman, 1994; Hansen et al., 2012; Vanderwende et al., 2016; Ghaisas et al., 2017; Xie and Archer, 2017), as well as wind farm effects downwind (Fitch et al., 2013a). Therefore, additional LES runs with stable and unstable conditions are needed to recalibrate the hybrid model for non-neutral conditions. Secondly, the hybrid model is based on the geometric model by Ghaisas and Archer (2016), which can be improved in several aspects, such as finding the optimal value for the maximum blockage distance L_∞, or including the lateral and vertical spread of the wake as a function of atmospheric stability.

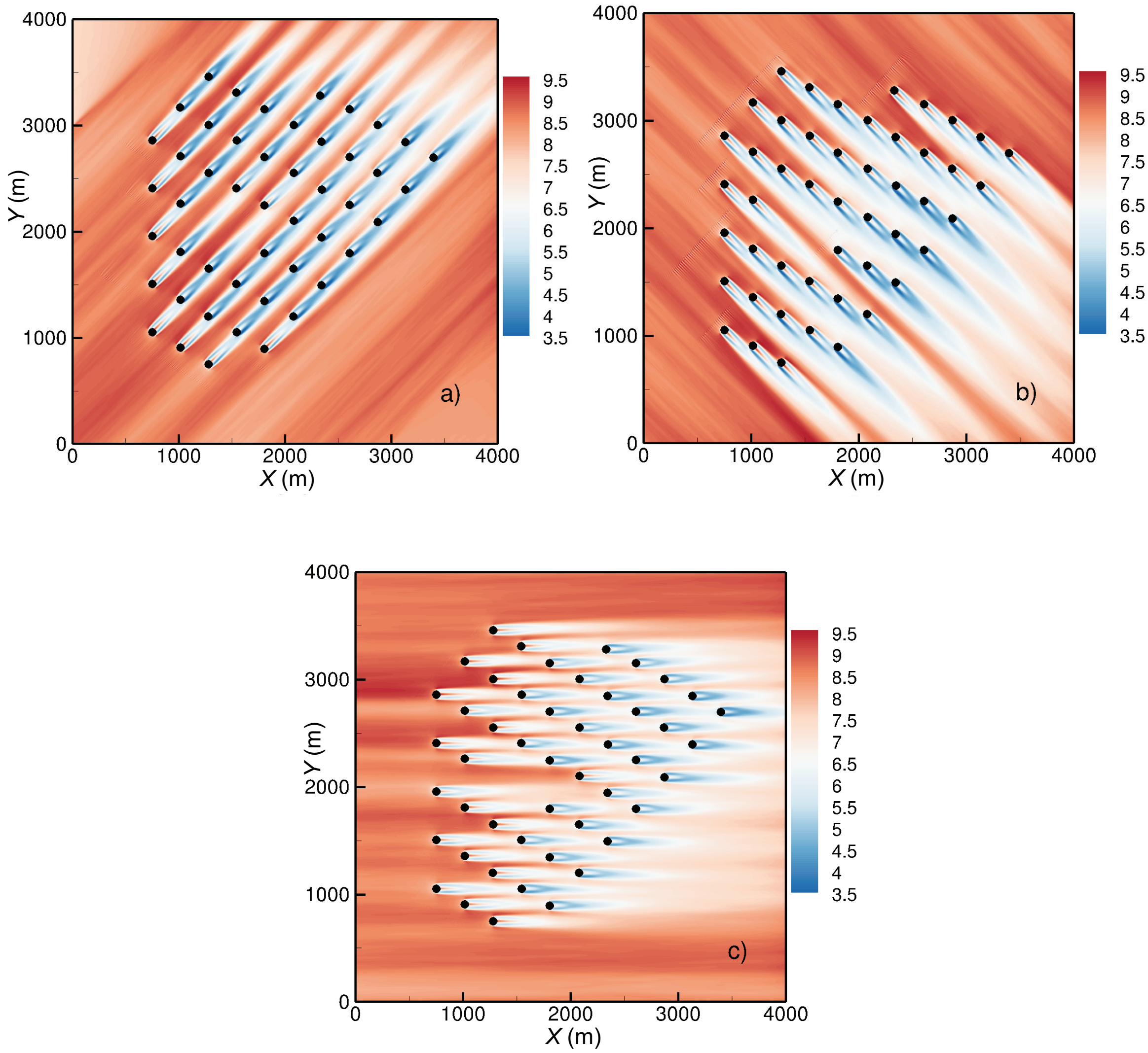

Figure 3.3: Contours of temporally-averaged horizontal velocity at hub height obtained from LES results of Lillgrund for (a) south-westerly (225°), (b) north-westerly (315°), and (c) westerly (270°) wind directions.

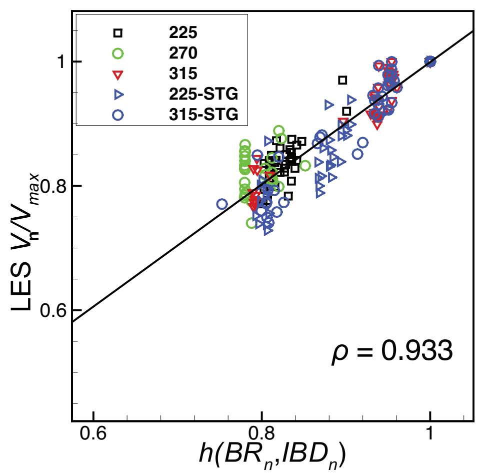

Figure 3.4: Normalized wind speed upstream of each turbine n from the five LES cases listed in Table 3.1 (y-axis) and from the proposed parameterization (x-axis); the black solid line is the one–one fit.

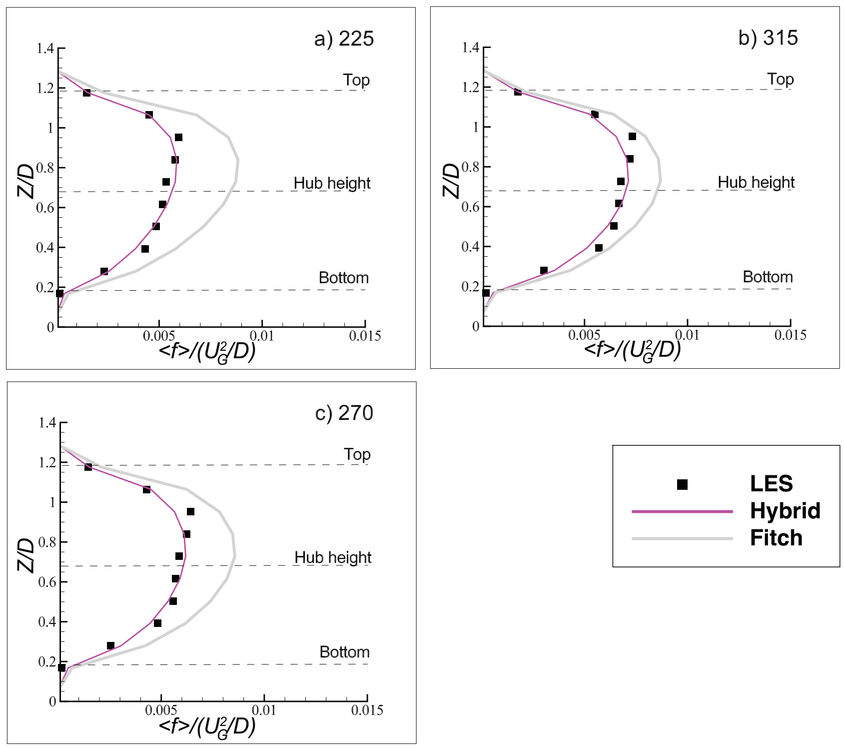

Figure 3.5: Vertical profiles of normalized turbine-induced body force $\langle \overline{f} \rangle$ predicted by the LES model, the Fitch model, and the hybrid model at Lillgrund for the (a) south-westerly (225°, (b) north-westerly (315°), and (c) westerly (270°) wind directions.

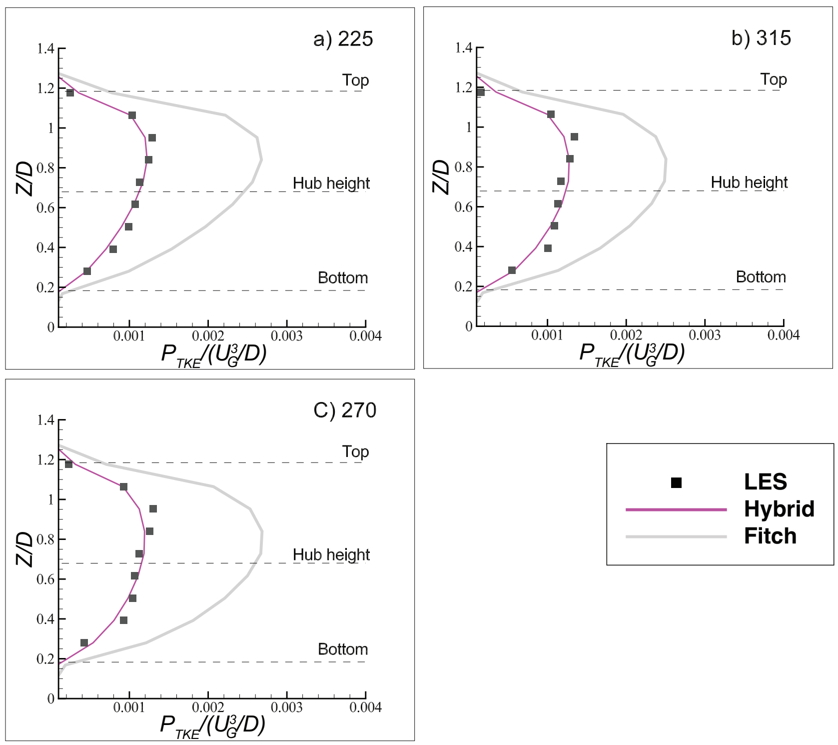

Figure 3.6: As Fig. 3.5, but for the turbine-induced TKE term P_{TKE}, normalized by the geostrophic wind speed U_G and the rotor diameter D.

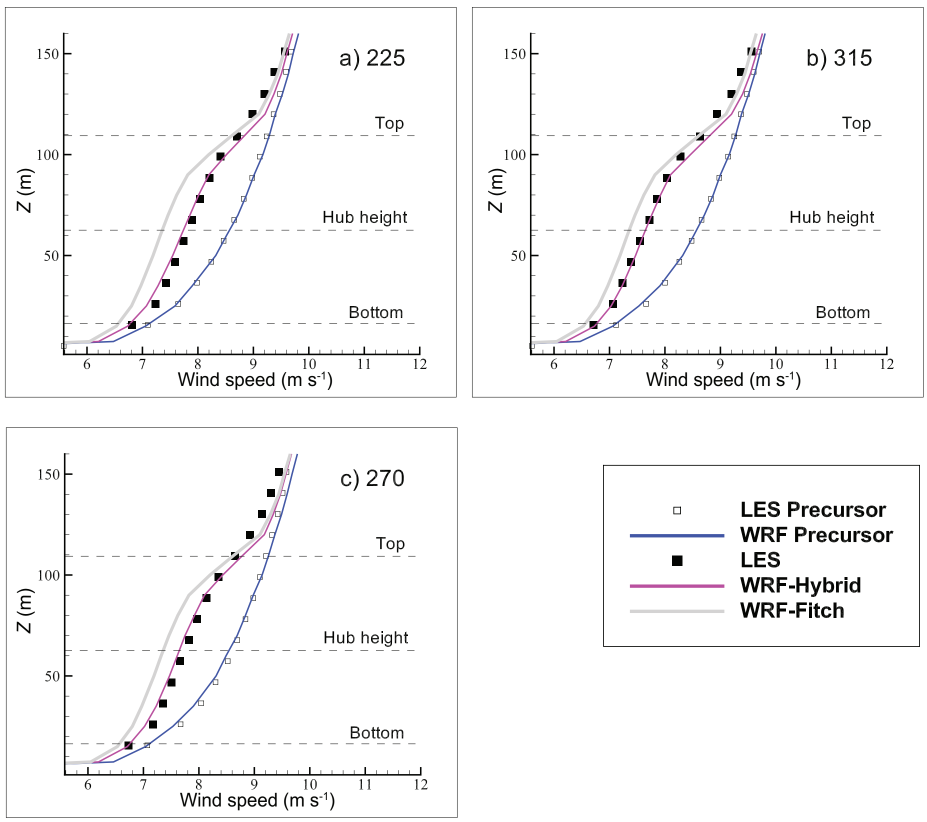

Figure 3.7: As for Fig. 3.5 but for wind speed. The results of the LES model without turbines (LES Precursor) and WRF model without turbines (WRF Precursor) are also shown.

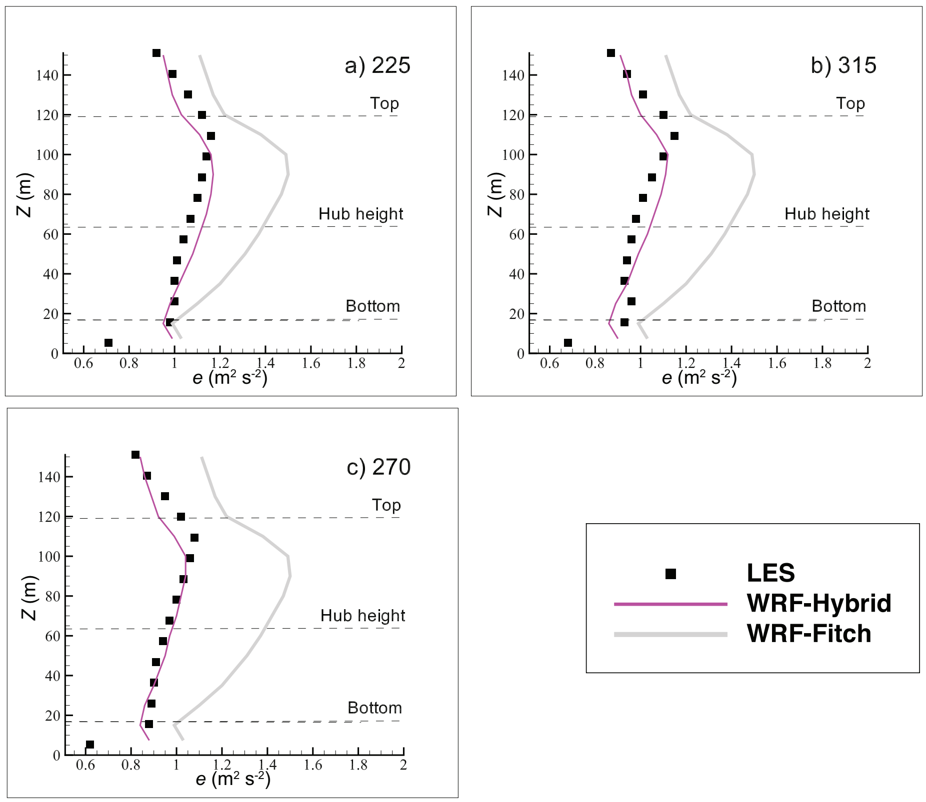

Figure 3.8: As in Figure 3.5, but for TKE.

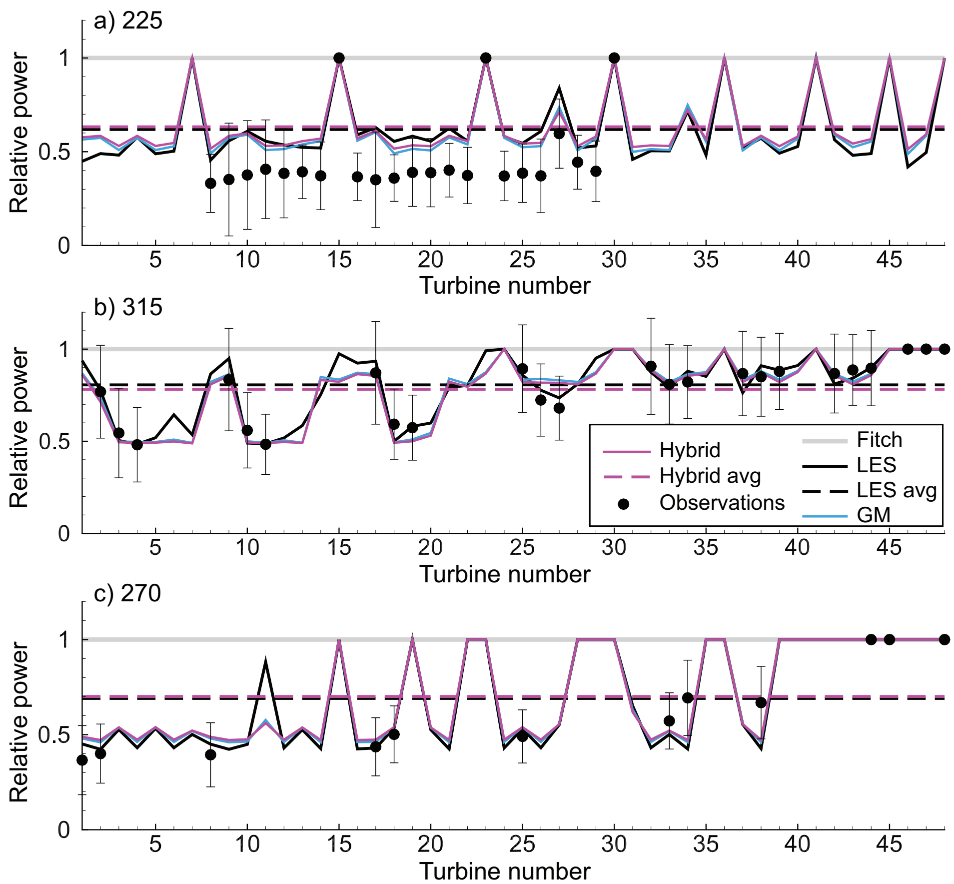

Figure 3.9: Relative power of the 48 wind turbines at Lillgrund calculated with the hybrid model in the WRF–hybrid model (Hybrid) compared with LES results, the geometric model (GM), the WRF–Fitch model (Fitch), and wind farm data (only a few turbines available) for the (a) south-westerly (225°), (b) north-westerly (315°), and (c) westerly (270°) wind directions; dashed lines show the average wind farm power from the LES and hybrid models.

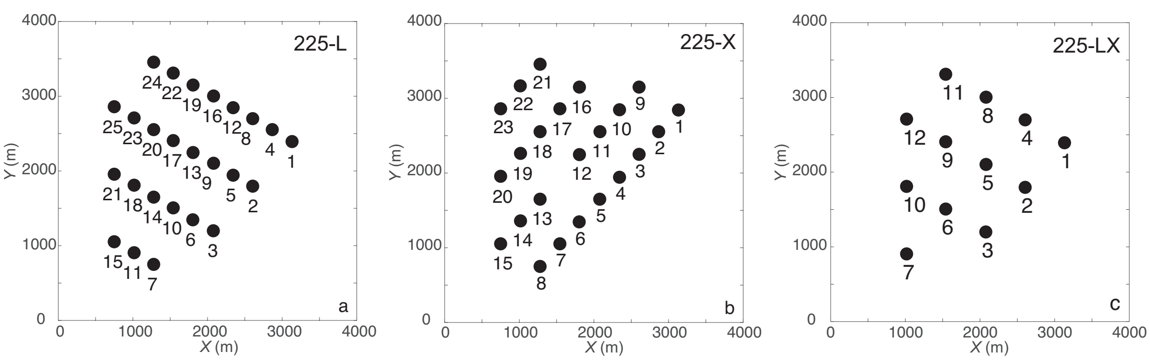

Figure 3.10: Layout of the additional three wind farms (Table 3.1) with similar areas as Lillgrund, but with double spacing for the (a) along-wind (225-L), (b) across-wind (225-X), and (c) along- and across-wind (225-LX) layouts in the prevailing south-westerly wind direction.

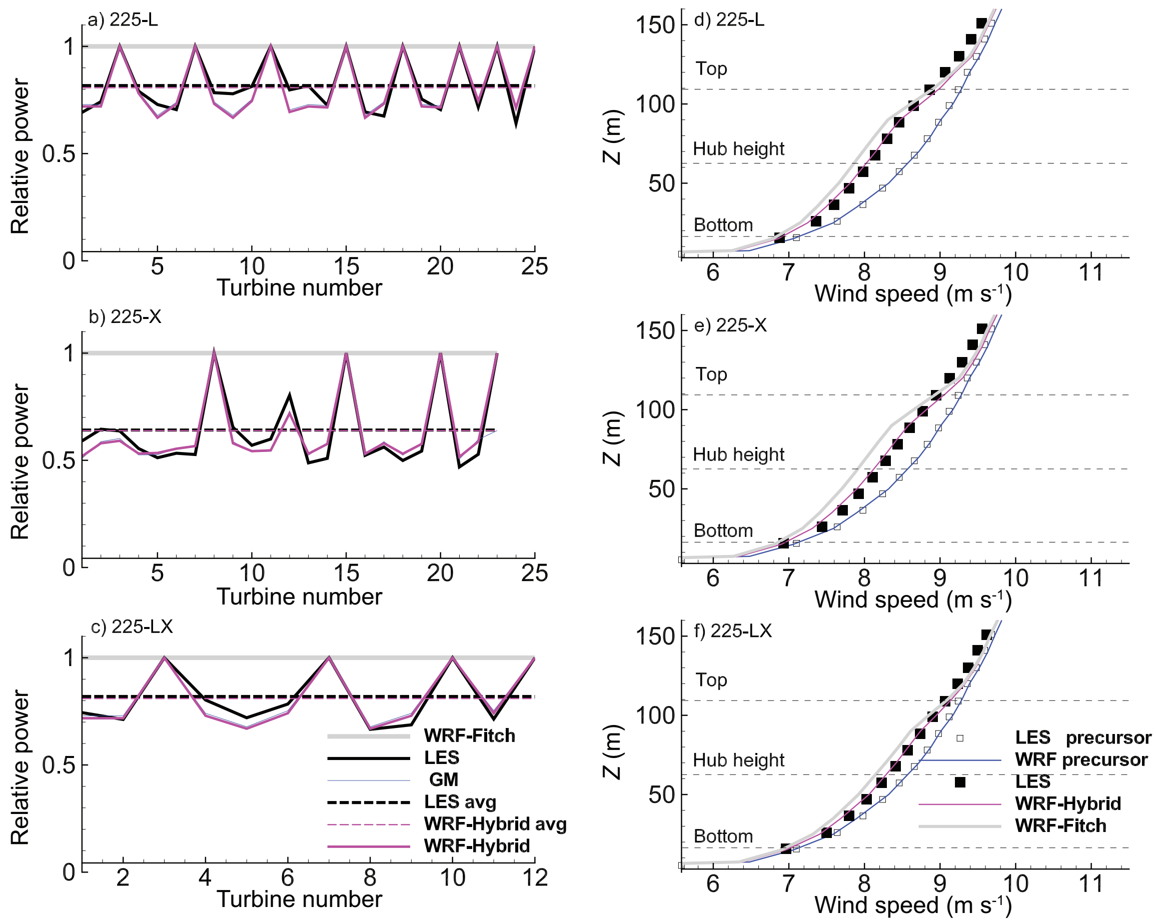

Figure 3.11: Relative power (left) and wind speed profiles (right) for the three double-spaced cases (Table 3.1) for the (a,d) 225-L, (b,e) 225-X, and (c,f) 225-LX layouts; dashed lines show the wind farm average power from the LES and hybrid models.

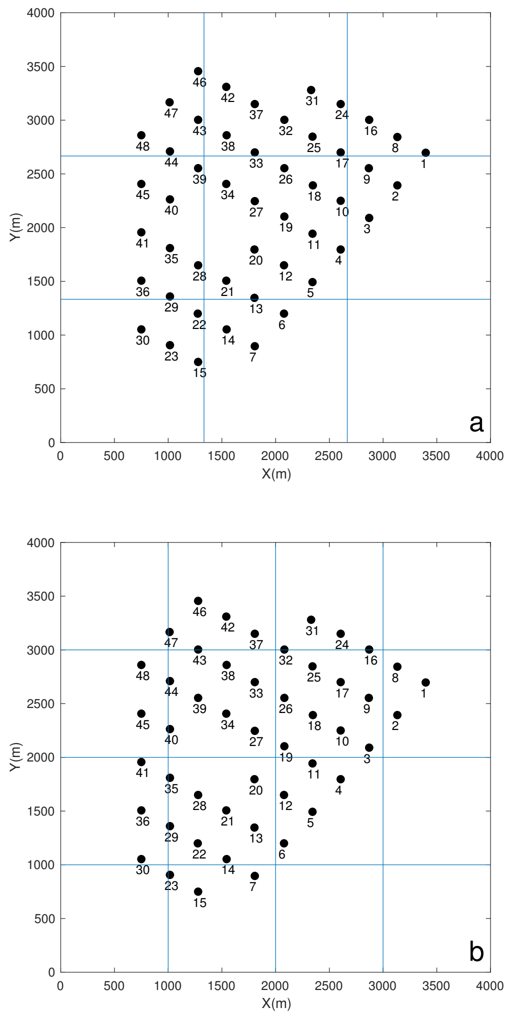

Figure 3.12: Turbine locations for different grid sizes, a) 9 grid cells b) 16 grid cells.

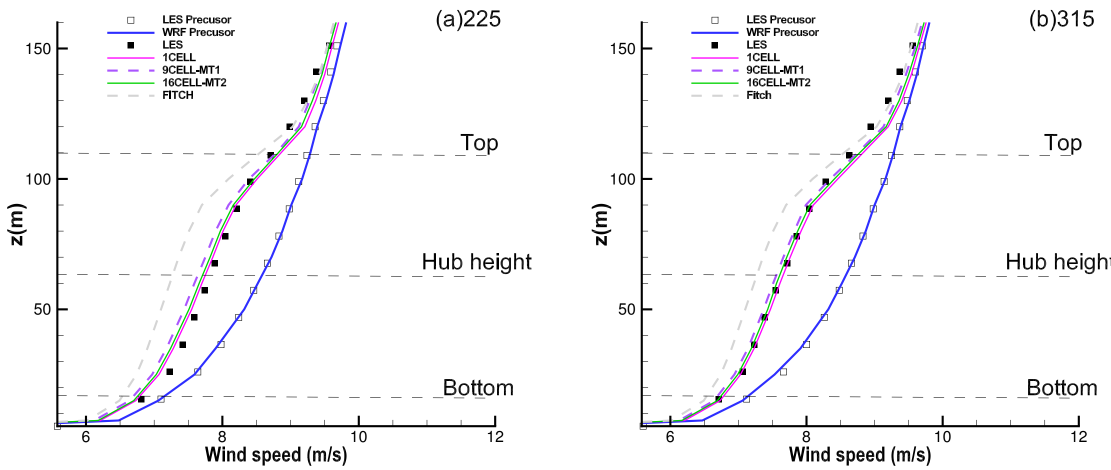

Figure 3.13: Same as Fig. 3.7, but with the single-cell results previously called "WRF-hybrid" labeled here as 1CELL. The two multi-grid methods (MT1 and MT2) are applied to the 3x3 and 4x4 grids, respectively, in the cases labeled as 9CELL-MT1 and 16CELL-MT2

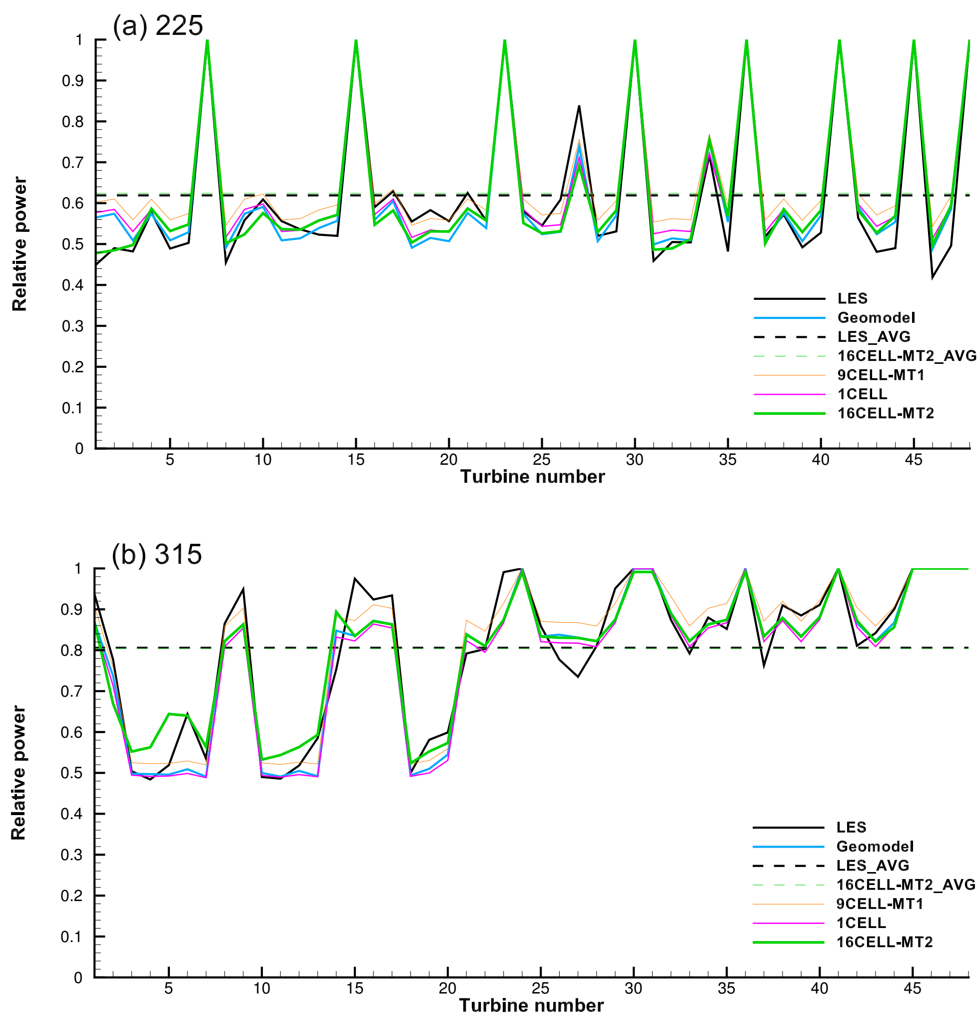

Figure 3.14: Relative power of the 48 wind turbines at Lillgrund calculated with the single-grid cell method (1CELL) and the two multi-grid methods (9CELL-MT1 and 16CELL-MT2), along with the wind-farm average from LES and from each case shown in Fig. 3.9.

Chapter 4
CONCLUSION

In this work, the impacts of large offshore wind farms on precipitation during hurricane Harvey are evaluated using the current wind farm parameterizations. A hybrid wind-farm parameterization is proposed and implemented in the WRF model.

Large-scale deployment of wind power can alter the precipitation pattern. During Hurricane Harvey, an obvious decrease in precipitation onshore and downstream of wind farms, and an increase in the offshore areas and upstream of and within wind farms is found. This can be explained by the changes in the horizontal divergence and vertical wind speed, which are essential for cloud formation. The sensitivity of the precipitation to different wind-farm layouts and wind-farm parameterizations has also been studied, confirming that offshore wind farms impact the precipitation distribution during a hurricane such as Harvey, regardless of the details of the wind-farm parameterization. The next phase of the study should be to identify the smallest array size that still has significant benefits using a more advanced and accurate wind-farm parameterization.

To improve the current wind-farm parameterization used in the WRF model, which is also employed to model the wind farms in previous chapters, a hybrid wind-farm parameterization is developed based on the results gained via the LES investigation, and the geometric properties of the wind-farm layout. The validation against both LES results and wind-farm data indicates that the hybrid parameterization performs well in terms of both the predicted vertical profiles of relevant physical properties, such as the wind speed and TKE, and the power production (within 10 percent). The validation of three artificial wind farms has also shown the ability to accommodate other configurations and other wind-farm layouts, regardless of the particular turbine spacing. The sensitivity test of different grid sizes confirms the model can handle larger wind farms occupying multiple grid cells.

BIBLIOGRAPHY

Abbasi S, Abbasi T, et al. (2016) Impact of wind-energy generation on climate: A rising spectre. Renewable and Sustainable Energy Reviews 59:1591–1598

Abkar M, Porté-Agel F (2013) The effect of free-atmosphere stratification on boundary-layer flow and power output from very large wind farms. Energies 6(5):2338–2361

Abkar M, Porté-Agel F (2015) A new wind-farm parameterization for large-scale atmospheric models. J Renew Sust Energy 7(1):013,121

Adams AS, Keith DW (2007) Wind energy and climate: Modeling the atmospheric impacts of wind energy turbines. In: Amer. Geophys. Union, San Francisco, B44B-08

Adams AS, Keith DW (2013) Are global wind power resource estimates overstated? Environ Res Lett 8(1):015,021

Ainslie JF (1988) Calculating the flowfield in the wake of wind turbines. J Wind Eng Ind Aerodyn 27(1):213–224

Aitken ML, Rhodes ME, Lundquist JK (2012) Performance of a Wind-Profiling Lidar in the Region of Wind Turbine Rotor Disks. J Atmos OceanTechnol 29(3):347–355

Aitken ML, Kosović B, Mirocha JD, Lundquist JK (2014) Large eddy simulation of wind turbine wake dynamics in the stable boundary layer using the weather research and forecasting model. J Renew Sust Energy 6(3):033,137

Archer CL, Mirzaeisefat S, Lee S (2013) Quantifying the sensitivity of wind farm performance to array layout options using large-eddy simulation. Geophys Res Lett 40(18):4963–4970

Archer CL, Wu S, Vasel-Be-Hagh A, Brodie JF, Delgado R, St Pé A, Oncley S, Semmer S (2018) Meteorological observations of wind turbine effects in the atmospheric boundary layer: The VERTEX field campaign. Bull Am Meteorol Soc (under review)

Armstrong A, Burton RR, Lee SE, Mobbs S, Ostle N, Smith V, Waldron S, Whitaker J (2016) Ground-level climate at a peatland wind farm in scotland is affected by wind turbine operation. Environ Res Lett 11(4):044,024

Baidya Roy S, Traiteur JJ (2010) Impacts of wind farms on surface air temperatures. Proc Natl Acad Sci (USA) 107(42):17,899–17,904

Baidya Roy S, Pacala S, Walko R (2004) Can large wind farms affect local meteorology? J Geophys Res Atmos 109(D19)

Banta RM, Pichugina YL, Brewer WA, Lundquist JK, Kelley ND, Sandberg SP, Alvarez RJI, Hardesty RM, Weickmann AM (2015) 3D volumetric analysis of wind turbine wake properties in the atmosphere using high-resolution Doppler lidar. J Atmos OceanTechnol 32(5):904–914

Barrie DB, Kirk-Davidoff DB (2010) Weather response to a large wind turbine array. Atmospheric Chemistry and Physics 10:769–775

Barthelmie RJ, Hansen K, Frandsen ST, Rathmann O, Schepers JG, Schlez W, Phillips J, Rados K, Zervos A, Politis ES, Chaviaropoulos PK (2009) Modelling and measuring flow and wind turbine wakes in large wind farms offshore. Wind Energy 12(5):431–444, DOI 10.1002/we.348, URL http://dx.doi.org/10.1002/we.348

Barthelmie RJ, Pryor S, Frandsen ST, Hansen KS, Schepers J, Rados K, Schlez W, Neubert A, Jensen L, Neckelmann S (2010) Quantifying the impact of wind turbine wakes on power output at offshore wind farms. J Atmos OceanTechnol 27(8):1302–1317

Bastankhah M, Porté-Agel F (2014) A new analytical model for wind-turbine wakes. Renew Energy 70:116–123

Bhaganagar K, Debnath M (2015) The effects of mean atmospheric forcings of the stable atmospheric boundary layer on wind turbine wake. J Renew Sust Energy 7(1):013,124

Blahak U, Goretzki B, Meis J (2010) A simple parameterization of drag forces induced by large wind farms for numerical weather prediction models. In: Proceedings of the European Wind Energy Conference & Exhibition

Brower M, Robinson N (2012) The openWind deep-array wake model: Development and validation. Tech. note, AWS Truepower

Calaf M, Meneveau C, Meyers J (2010) Large eddy simulation study of fully developed wind-turbine array boundary layers. Phys Fluids 22(1):015,110

Cavallo SM, Torn RD, Snyder C, Davis C, Wang W, Done J (2013) Evaluation of the advanced hurricane WRF data assimilation system for the 2009 atlantic hurricane season. Mon Wea Rev 141(2):523–541

Chamorro LP, Porté-Agel F (2010) Effects of thermal stability and incoming boundary-layer flow characteristics on wind-turbine wakes: a wind-tunnel study. Boundary-Layer Meteorol 136:515–533

Churchfield J, Lee S, Michalakes J, Moriarty PJ (2012a) A numerical study of the effects of atmospheric and wake turbulence on wind turbine dynamics. J Turbul 13(14):1–32

Churchfield , Lee S, Moriarty P, Martinez L, Leonardi S, Vijayakumar G, Brasseur J (2012b) A large-eddy simulations of wind-plant aerodynamics. In: 50th AIAA Aerospace Sciences Meeting, p 537

Creech A, Früh WG, Maguire AE (2015) Simulations of an offshore wind farm using large-eddy simulation and a torque-controlled actuator disc model. Surveys in Geophysics 36(3):427–481

Dahlberg JÅ (2009) Assessment of the Lillgrund windfarm. Tech. Rep. 6_1 LG Pilot Report, Vattenfall

Dodla VB, Desamsetti S, Yerramilli A (2011) A comparison of HWRF, ARW and NMM models in hurricane Katrina (2005) simulation. International journal of environmental research and public health 8(6):2447–2469

Ek M, Mitchell K, Lin Y, Grunmann P, Rogers E, Gayno G, Koren V, Tarpley J (2003) Implementation of the upgraded Noah land-surface model in the NCEP operational mesoscale Eta model. J Geophys Res 108:8851

Eriksson O, Lindvall J, Breton SP, Ivanell S (2015) Wake downstream of the Lillgrund wind farm - A comparison between LES using the actuator disc method and a wind farm parametrization in WRF. In: J. Phys.: Conf. Ser., IOP Publishing, vol 625, pp 012–028

España G, Aubrun S, Loyer S, Devinant P (2011) Spatial study of the wake meandering using modelled wind turbines in a wind tunnel. Wind Energy 14(7):923–937, DOI 10.1002/we.515

Fiedler B, Bukovsky M (2011) The effect of a giant wind farm on precipitation in a regional climate model. Environ Res Lett 6(4):045,101

Fitch AC (2015) Climate impacts of large-scale wind farms as parameterized in a global climate model. Journal of Climate 28(15):6160–6180

Fitch AC, Olson JB, Lundquist JK, Dudhia J, Gupta AK, Michalakes J, Barstad I (2012) Local and mesoscale impacts of wind farms as parameterized in a mesoscale NWP model. Mon Wea Rev 140(9):3017–3038

Fitch AC, Lundquist JK, Olson JB (2013a) Mesoscale influences of wind farms throughout a diurnal cycle. Mon Wea Rev 141(7):2173–2198

Fitch AC, Olson JB, Lundquist JK (2013b) Parameterization of wind farms in climate models. J Clim 26(17):6439–6458

Flood Warning System (FWS) (2017) Harris county flood control district rainfall. https://www.harriscountyfws.org, accessed 2018-01-15

Frandsen S, Barthelmie R, Pryor S, Rathmann O, Larsen S, Højstrup J, Thøgersen M (2006) Analytical modelling of wind speed deficit in large offshore wind farms. Wind Energy 9(1-2):39–53

Ghaisas NS, Archer CL (2016) Geometry-based models for studying the effects of wind farm layout. J Atmos OceanTechnol 33(3):481–501, DOI 10.1175/JTECH-D-14-00199.1

Ghaisas NS, Archer CL, Xie S, Wu S, Maguire E (2017) Evaluation of layout and atmospheric stability effects in wind farms using large-eddy simulation. Wind Energy DOI 10.1002/we.2091

GWEC GWEC (2014) Global wind statistics 2013

Hamill TM, Whitaker JS, Fiorino M, Benjamin SG (2011) Global ensemble predictions of 2009s tropical cyclones initialized with an ensemble Kalman filter. Mon Wea Rev 139(2):668–688

Hansen KS, Barthelmie RJ, Jensen LE, Sommer A (2012) The impact of turbulence intensity and atmospheric stability on power deficits due to wind turbine wakes at Horns Rev wind farm. Wind Energy 15(1):183–196

Iungo GV, Wu YT, , Porté-Agel F (2013) Field measurements of wind turbine wakes with lidars. J Atmos OceanTechnol 30:274–287

Jacobson MZ, Archer CL (2012) Saturation wind power potential and its implications for wind energy. Proc Natl Acad Sci (USA) 109(39):15,679–15,684

Jacobson MZ, Archer CL, Kempton W (2014) Taming hurricanes with arrays of offshore wind turbines. Nat Clim Change 4(3):195–200

Jensen NO (1983) A note on wind generator interaction. Tech. Note Risø-M-2411, Risø National Laboratory, Denmark

Jiménez PA, Navarro J, Palomares AM, Dudhia J (2015) Mesoscale modeling of offshore wind turbine wakes at the wind farm resolving scale: a composite-based analysis with the Weather Research and Forecasting model over Horns Rev. Wind Energy 18:559–566

Johnstone R, Coleman GN (2012) The turbulent ekman boundary layer over an infinite wind-turbine array. Journal of Wind Engineering and Industrial Aerodynamics 100(1):46–57

Kain J, Fritsch J (1992) The role of the convective trigger function in numerical forecasts of mesoscale convective systems. Meteor Atmos Phys 49(1):93–106

Kain JS (2004) The Kain–Fritsch convective parameterization: an update. J Appl Meteor Climatol 43(1):170–181

Katic I, Højstrup J, Jensen NO (1986) A simple model for cluster efficiency. In: European Wind Energy Association Conference and Exhibition, pp 407–410

Keith DW, DeCarolis JF, Denkenberger DC, Lenschow DH, Malyshev SL, Pacala S, Rasch PJ (2004) The influence of large-scale wind power on global climate. Proc Natl Acad Sci (USA) 101(46):16,115–16,120

Kirk-Davidoff DB, Keith DW (2008) On the climate impact of surface roughness anomalies. J Atmos Sci 65(7):2215–2234

Kurihara Y, Bender MA, Tuleya RE, Ross RJ (1995) Improvements in the GFDL hurricane prediction system. Mon Wea Rev 123(9):2791–2801

Larsen GC (1988) A simple wake calculation procedure. Tech. Note Risø-M-2760, Risø National Laboratory, Denmark

Larsen GC, Madsen Aagaard H, Bingöl F, Mann J, Ott S, Sørensen JN, Okulov V, Troldborg N, Nielsen NM, Thomsen K, Larsen TJ, Mikkelsen R (2007) Dynamic wake meandering modeling. Tech. Rep. Risø-R-1607(EN), Risø National Laboratory

Lu H, Porté-Agel F (2011) Large-eddy simulation of a very large wind farm in a stable atmospheric boundary layer. Phys Fluids 23(6):065,101

Lu H, Porté-Agel F (2015) On the impact of wind farms on a convective atmospheric boundary layer. Boundary-Layer Meteorol 157(1):81–96

Madsen HA, Larsen GC, Larsen TJ, Troldborg N, Mikkelsen R (2010) Calibration and validation of the dynamic wake meandering model for implementation in an aeroelastic code. J Sol Energy Eng 132(4):041,014

Magnusson M, Smedman AS (1994) Influence of atmospheric stability on wind turbine wakes. Wind Eng 18(3):139–152

Marvel K, Kravitz B, Caldeira K (2013a) Geophysical limits to global wind power. Nature Climate Change 3(2):118

Marvel K, Kravitz B, Caldeira K (2013b) Geophysical limits to global wind power. Nat Clim Change 3:118–121

Mellor GL, Yamada T (1974) A hierarchy of turbulence closure models for planetary boundary layers. J Atmos Sci 31(7):1791–1806

Mellor GL, Yamada T (1982) Development of a turbulence closure model for geophysical fluid problems. Rev Geophys 20(4):851–875

Miller LM, Gans F, Kleidon A (2011) Estimating maximum global land surface wind power extractability and associated climatic consequences. Earth Syst Dynam 2(1):1–12

Mirocha J, Kosovic B, Aitken M, Lundquist J (2014) Implementation of a generalized actuator disk wind turbine model into the weather research and forecasting model for large-eddy simulation applications. J Renew Sust Energy 6(1):013,104

Mirocha JD, Rajewski DA, Marjanovic N, Lundquist JK, Kosović B, Draxl C, Churchfield MJ (2015) Investigating wind turbine impacts on near-wake flow using profiling lidar data and large-eddy simulations with an actuator disk model. J Renew Sust Energy 7(4):043,143

Nakanishi M, Niino H (2009) Development of an improved turbulence closure model for the atmospheric boundary layer. Meteor Soc Japan 87(5):895–912

Ott S (2011) Linearised CFD models for wakes. Tech. Rep. Risø-R-1772(EN), Risø National Laboratory

Pan Y, Archer CL (2018) A hybrid wind farm parameterization for mesoscale and climate models. Boundary-Layer Meteorol DOI 10.1007/s10546-018-0351-9

Pope SB (2000) Turbulent Flows. Cambridge University Press

Porté-Agel F, Wu YT, Lu H, Conzemius RJ (2011) Large-eddy simulation of atmospheric boundary layer flow through wind turbines and wind farms. J Wind Eng Ind Aerodyn 99(4):154–168

Possner A, Caldeira K (2017) Geophysical potential for wind energy over the open oceans. Proc Natl Acad Sci (USA) 114(43):11,338–11,343

Rajewski DA, Takle ES, Lundquist JK, Oncley S, Prueger JH, Horst TW, Rhodes ME, Pfeiffer R, Hatfield JL, Spoth KK, et al. (2013) Crop wind energy experiment (CWEX): Observations of surface-layer, boundary layer, and mesoscale interactions with a wind farm. Bull Amer Meteor Soc 94(5):655–672

Rajewski DA, Takle ES, Lundquist JK, Prueger JH, Pfeiffer RL, Hatfield JL, Spoth KK, Doorenbos RK (2014) Changes in fluxes of heat, H_2O, and CO_2 caused by a large wind farm. Agric For Meteor 194:175–187

Shen WZ, Sørensen J (2002) Numerical modeling of wind turbine wakes. J Fluids Eng 124(2):393–399

Skamarock WC, Klemp JB, Dudhia J, Gill DO, Barker DM, Duda MG, Huang XY, Wang W, Powers JG (2008) A description of the Advanced Research WRF version 3. Tech. Rep. NCAR/TN-475+STR, National Center for Atmospheric Research

Smagorinsky J (1963) General circulation experiments with the primitive equations: I. the basic experiment*. Mon Wea Rev 91(3):99–164

Smith CM, Barthelmie R, Pryor S (2013) In situ observations of the influence of a large onshore wind farm on near-surface temperature, turbulence intensity and wind speed profiles. Environ Res Lett 8(3):034,006

Somnath Baidya R (2011) Simulating impacts of wind farms on local hydrometeorology. J Wind Eng Ind Aerodyn 99(4):491–498

Sorensen P, Nielsen T (2006) Recalibrating wind turbine wake model parametersvalidating the wake model performance for large offshore wind farms. In: European Wind Energy Conference and Exhibition, EWEA

Stevens RJ, Gayme DF, Meneveau C (2014) Large eddy simulation studies of the effects of alignment and wind farm length. Journal of Renewable and Sustainable Energy 6(2):023,105

The Weather Company (TWC) (2017) Harvey's historical track. https://weather.com/storms/hurricane-central/harvey-2017/AL092017, accessed 2018-01-15

Troldborg N, Sørensen JN, Mikkelsen R, Sørensen NN (2014) A simple atmospheric boundary layer model applied to large eddy simulations of wind turbine wakes. Wind Energy 17(4):657–669

US Energy Information Administration (2016) International energy outlook 2016. https://www.eia.gov/outlooks/archive/ieo16/, accessed 2018-05-23

US Energy Information Administration (2017) Wind turbines provide 8% of U.S. generating capacity, more than any other renewable source. https://www.eia.gov/todayinenergy/detail.php?id=31032#, accessed 2017-12-22

Vanderwende BJ, Kosović B, Lundquist JK, Mirocha JD (2016) Simulating effects of a wind-turbine array using les and rans. J Adv Model Earth Syst 8(3):1376–1390

Vautard R, Thais F, Tobin I, Bréon FM, De Lavergne JgD, Colette A, Yiou P, Ruti PM (2014) Regional climate model simulations indicate limited climatic impacts by operational and planned european wind farms. Nature communications 5

Volker P, Badger J, Hahmann AN, Ott S (2015) The explicit wake parametrisation v1.0: A wind farm parametrisation in the mesoscale model WRF. Geosci Model Dev 8(11):3715–3731

Vollmer L, Steinfeld G, Heinemann D, Kühn M (2016) Estimating the wake deflection downstream of a wind turbine in different atmospheric stabilities: an les study. Wind Energy Science 1(2):129–141

Wang C, Prinn RG (2010) Potential climatic impacts and reliability of very large-scale wind farms. Atmospheric Chemistry and Physics 10(4):2053–2061

Wang Y (1998) On the bogusing of tropical cyclones in numerical models: The influence of vertical structure. Meteor Atmos Phys 65(3):153–170

Wu YT, Porté-Agel F (2011) Large-eddy simulation of wind-turbine wakes: Evaluation of turbine parametrisations. Boundary-Layer Meteorol 138(3):345–366

Wu YT, Porté-Agel F (2013) Simulation of turbulent flow inside and above wind farms: model validation and layout effects. Boundary-Layer Meteorol 146(2):1–25

Wu YT, Porté-Agel F (2015) Modeling turbine wakes and power losses within a wind farm using les: An application to the horns rev offshore wind farm. Renew Energy 75:945–955

Xie S, Archer C (2015) Self-similarity and turbulence characteristics of wind turbine wakes via large-eddy simulation. Wind Energy 18(10):1815–1838

Xie S, Archer CL (2017) A numerical study of wind-turbine wakes for three atmospheric stability conditions. Boundary-Layer Meteorol DOI 10.1007/s10546-017-0259-9

Zhang F, Weng Y, Sippel JA, Meng Z, Bishop CH (2009) Cloud-resolving hurricane initialization and prediction through assimilation of doppler radar observations with an ensemble Kalman filter. Mon Wea Rev 137(7):2105–2125

Zhang F, Weng Y, Gamache JF, Marks FD (2011) Performance of convection-permitting hurricane initialization and prediction during 2008–2010 with ensemble data assimilation of inner-core airborne doppler radar observations. Geophys Res Lett 38(15)

Zhang W, Markfort CD, Porté-Agel F (2013) Experimental study of the impact of large-scale wind farms on land–atmosphere exchanges. Environmental Research Letters 8(1):015,002

Zhou L, Tian Y, Roy SB, Thorncroft C, Bosart LF, Hu Y (2012) Impacts of wind farms on land surface temperature. Nat Clim Change 2(7):539–543

Appendix

COPYRIGHT PERMISSION

SPRINGER NATURE LICENSE
TERMS AND CONDITIONS

Jul 11, 2018

This Agreement between yang pan ("You") and Springer Nature ("Springer Nature") consists of your license details and the terms and conditions provided by Springer Nature and Copyright Clearance Center.

License Number	4384790119238
License date	Jul 09, 2018
Licensed Content Publisher	Springer Nature
Licensed Content Publication	Boundary Layer Meteorology
Licensed Content Title	A Hybrid Wind-Farm Parametrization for Mesoscale and Climate Models
Licensed Content Author	Yang Pan, Cristina L. Archer
Licensed Content Date	Jan 1, 2018
Type of Use	Thesis/Dissertation
Requestor type	academic/university or research institute
Format	print and electronic
Portion	full article/chapter
Will you be translating?	no
Circulation/distribution	<501
Author of this Springer Nature content	yes
Title	phd dissertation
Instructor name	CRISTINA ARCHER
Institution name	university of delaware
Expected presentation date	Jul 2018
Order reference number	0001
Requestor Location	yang pan 400 stamford dr NEWARK, DE 19711 United States Attn: yang pan
Billing Type	Invoice
Billing Address	yang pan 400 stamford dr NEWARK, DE 19711 United States Attn: yang pan
Total	0.00 USD

Terms and Conditions

Springer Nature Terms and Conditions for RightsLink Permissions

Springer Customer Service Centre GmbH (the Licensor) hereby grants you a non-exclusive, world-wide licence to reproduce the material and for the purpose and requirements specified in the attached copy of your order form, and for no other use, subject to the conditions below:

1. The Licensor warrants that it has, to the best of its knowledge, the rights to license reuse of this material. However, you should ensure that the material you are requesting is original to the Licensor and does not carry the copyright of another entity (as credited in the published version).

   If the credit line on any part of the material you have requested indicates that it was reprinted or adapted with permission from another source, then you should also seek permission from that source to reuse the material.

2. Where **print only** permission has been granted for a fee, separate permission must be obtained for any additional electronic re-use.

3. Permission granted **free of charge** for material in print is also usually granted for any electronic version of that work, provided that the material is incidental to your work as a whole and that the electronic version is essentially equivalent to, or substitutes for, the print version.

4. A licence for 'post on a website' is valid for 12 months from the licence date. This licence does not cover use of full text articles on websites.

5. Where **'reuse in a dissertation/thesis'** has been selected the following terms apply: Print rights for up to 100 copies, electronic rights for use only on a personal website or institutional repository as defined by the Sherpa guideline (www.sherpa.ac.uk/romeo/).

6. Permission granted for books and journals is granted for the lifetime of the first edition and does not apply to second and subsequent editions (except where the first edition permission was granted free of charge or for signatories to the STM Permissions Guidelines http://www.stm-assoc.org/copyright-legal-affairs/permissions/permissions-guidelines/), and does not apply for editions in other languages unless additional translation rights have been granted separately in the licence.

7. Rights for additional components such as custom editions and derivatives require additional permission and may be subject to an additional fee. Please apply to Journalpermissions@springernature.com/bookpermissions@springernature.com for these rights.

8. The Licensor's permission must be acknowledged next to the licensed material in print. In electronic form, this acknowledgement must be visible at the same time as the figures/tables/illustrations or abstract, and must be hyperlinked to the journal/book's homepage. Our required acknowledgement format is in the Appendix below.

9. Use of the material for incidental promotional use, minor editing privileges (this does not include cropping, adapting, omitting material or any other changes that affect the meaning, intention or moral rights of the author) and copies for the disabled are permitted under this licence.

10. Minor adaptations of single figures (changes of format, colour and style) do not require the Licensor's approval. However, the adaptation should be credited as shown in Appendix below.

Appendix — Acknowledgements:

For Journal Content:

Reprinted by permission from [**the Licensor**]: [**Journal Publisher** (e.g.